



**HAL**  
open science

# Geomorphology of a modern carbonate slope system and associated sedimentary processes: Example of the giant Great Abaco Canyon, Bahamas

Audrey Recouvreur, Natacha Fabregas, Thierry Mulder, Vincent Hanquiez, Kelly Fauquembergue, Elsa Tournadour, Hervé Gillet, Jean Borgomano, Emmanuelle Poli, Jean-baptiste Kucharski, et al.

## ► To cite this version:

Audrey Recouvreur, Natacha Fabregas, Thierry Mulder, Vincent Hanquiez, Kelly Fauquembergue, et al.. Geomorphology of a modern carbonate slope system and associated sedimentary processes: Example of the giant Great Abaco Canyon, Bahamas. *Sedimentology*, 2021, 68 (1), pp.266-293. 10.1111/sed.12777 . hal-03046901

**HAL Id: hal-03046901**

**<https://hal.science/hal-03046901v1>**

Submitted on 21 May 2024

**HAL** is a multi-disciplinary open access archive for the deposit and dissemination of scientific research documents, whether they are published or not. The documents may come from teaching and research institutions in France or abroad, or from public or private research centers.

L'archive ouverte pluridisciplinaire **HAL**, est destinée au dépôt et à la diffusion de documents scientifiques de niveau recherche, publiés ou non, émanant des établissements d'enseignement et de recherche français ou étrangers, des laboratoires publics ou privés.

## Geomorphology of a modern carbonate slope system and associated sedimentary processes: Example of the giant Great Abaco Canyon, Bahamas

Recouvreur Audrey <sup>1,\*</sup>, Fabregas Natacha <sup>2</sup>, Mulder Thierry <sup>1</sup>, Hanquiez Vincent <sup>1</sup>, Fauquembergue Kelly <sup>1</sup>, Tournadour Elsa <sup>3,4</sup>, Gillet Hervé <sup>1</sup>, Borgomano Jean <sup>5</sup>, Poli Emmanuelle, Kucharski Jean-baptiste <sup>1</sup>, Wilk Stanislas <sup>1</sup>

<sup>1</sup> Université de Bordeaux EPOC UMR 5805 33615 Pessac Cedex ,France

<sup>2</sup> Department of Earth Science University of Bergen Allégaten 41 5007 Bergen ,Norway

<sup>3</sup> IFREMER Géosciences Marines CS 10070, 29280 Plouzané, France

<sup>4</sup> Geological Survey of New Caledonia DIMENC BP 465 98845 Nouméa New Caledonia ,France

<sup>5</sup> Centre Européen de Recherche et d'Enseignement de Géosciences de l'Environnement Aix-Marseille Université – CNRS (UMR7330) – IRD (UMR 161) – COLLEGE de France – USC INRA – OSU – Institut PYTHEAS – Technopole Environnement Arbois-Méditerranée BP80 13545 Aix en Provence Marseille CEDEX 04 ,France

\* Corresponding author : Audrey Recouvreur , email address : [audrey.recouvreur@gmail.com](mailto:audrey.recouvreur@gmail.com)

### Abstract :

The large acoustic data set acquired during the Carambar cruises is composed of high resolution bathymetry, backscatter data and very-high resolution seismic lines which allow for an overview of the morphology and sediment transfer processes from the shallow upper slope to the abyssal plain of a modern carbonate system: the north-eastern slope of the Little Bahama Bank. Surficial distribution of the acoustic facies and echofacies reflects a wide variety of sedimentary processes along and across the slope. The western sector of the Little Bahama Bank is dominated by depositional processes whereas its eastern sector, which is incised in the lower slope by giant canyons, is affected by erosion and bypass processes. Datasets suggest that currents play an important role both along-slope sedimentary processes and in the abyssal plain. The Antilles Current appears to affect a large part of the middle and lower slopes. The absence of sizable present-day channel/levée complexes or lobes at the mouth of the canyon – revealed by the bathymetric map – indicates that the southward flowing Deep Western Boundary Current influences modern abyssal sediment deposition. Based on depositional processes and indicators of canyon maturity observed in facies distribution, the current study proposes that differential subsidence affects the eastern versus western part of the bank. The morphology of the Great Abaco Canyon and Little Abaco Canyon, which extends parallel to the platform, and the Little Bahama Bank slope appears to be related to the Great Abaco Fracture Zone.

**Keywords :** Backscatter Bahamas, carbonate slope, echofacies, giant canyon, sea floor morphology, sedimentary processes

58 **INTRODUCTION**

59 Submarine canyons are structures incising the continental margins or shelves with a width and height of up  
60 to several kilometres (Shepard & Dill, 1966). Acting as catalysts of sediment export from shelves towards  
61 the deeper basin via their steep flanks, submarine canyons are critical elements of basin sedimentary  
62 deposits. Studies on submarine canyons have focused on siliciclastic systems (Babonneau *et al.*, 2002;  
63 Paull *et al.*, 2013; Tubau *et al.*, 2015), which are more attractive in terms of reservoir potential for  
64 hydrocarbons. Recent industrial discoveries in carbonate slopes (Bertello *et al.*, 2010; Busson *et al.*, 2019)  
65 have boosted their attractiveness and hence have piqued the scientific interest of such systems. However,  
66 sedimentary processes affecting purely carbonate canyons, rivaling siliciclastic canyons in terms of size,  
67 and their impact on carbonate sediment transfers and sources remain poorly understood. The Little Abaco  
68 Canyon and especially the Great Abaco Canyon have only been briefly described in the past decades  
69 (Shepard & Dill, 1966; Benson *et al.*, 1978; Mullins & Neumann, 1979; Mulder *et al.*, 2018).

70 As the Bahamian carbonate platform is one of the best-known modern carbonate systems, the  
71 Carambar cruises have targeted its slopes and associated incising canyons. Previous Carambar (2010) and  
72 Carambar 1.5 (2014) oceanographic cruises imaged a large part of the Little Bahama Bank (LBB) north-  
73 west slope using multibeam echo-sounder data and very-high resolution seismic profiles (Fig. 1; Mulder *et*  
74 *al.*, 2012a, 2014, 2017b). These studies have focused on: (i) the LBB periplatform drift, (Chabaud, 2016);  
75 (ii) the architecture of the slope canyons and mass transport complexes affecting the eastern LBB (Mulder  
76 *et al.*, 2012a; Tournadour, 2015, 2017); (iii) the genesis and growth of the carbonate wedge along the LBB  
77 (Fauquembergue *et al.*, 2018); and (iv) sediment transfers across the LBB slope (Tournadour, 2015;  
78 Fauquembergue, 2018). In order to provide a holistic view of the carbonate system, the consideration of the  
79 region as a whole has yet to integrate the complete study of the two main canyons present in the zone: the  
80 Great Abaco Canyon and the Little Abaco Canyon.

81 New high-resolution multibeam bathymetry, backscatter and very-high resolution seismic data  
82 acquired during the Carambar 2 (2016 to 2017) cruise enabled visualization of the eastern half of the slope  
83 of the modern LBB from shallow to deep environments (Fig. 1). The bathymetry of the eastern sector has  
84 highlighted the presence of two giant canyons previously described by Mulder *et al.* (2018): the Great  
85 Abaco Canyon (GAC) and the Little Abaco Canyon (LAC). The present study is based on a combination of  
86 acoustic data that provide a large-scale view of sedimentary distribution, something that is difficult to  
87 recognize if only using sedimentary data.

88 This approach allows the potential links between: (i) the sedimentary surface and subsurface processes;  
89 and (ii) slope structure to be highlighted. This paper explains that the connectivity of these elements is  
90 based on carbonate transfer from the slope to the ultra-deep domain through potentially structurally

91 controlled canyons. The work here also provides knowledge regarding giant purely carbonate canyons  
92 which are disconnected from the platform, along with comprehensive elements on how they work both in  
93 terms of source and transfer of carbonate material to the basin.

## 94 **REGIONAL SETTINGS**

### 95 **Physiography and oceanography**

96 The Bahamian platforms form an almost pure marine carbonate sedimentary system isolated from the  
97 siliciclastic terrigenous continental input by deep channels and escarpments. Platforms, slopes and the  
98 abyssal plain developed over a wide marine area (over 32 000 km<sup>2</sup>) which is supplied by a tropical  
99 carbonate factory (Schlager, 2005). The archipelago is located on the western margin of the Atlantic Ocean.  
100 Covering more than 300 000 km<sup>2</sup>, this archipelago is composed of more than 700 islands and is bordered by  
101 the Blake Bahama Escarpment to the east (BBE; Buchan, 2000), the contouritic Blake Plateau (BP) to the  
102 north, the Old Bahama Channel to the south and the Florida Strait to the west (Fig. 1). Several islands are  
103 developed in the north and centre of the Bahamas on two large carbonate platforms, the Little Bahama  
104 Bank (LBB) and the Great Bahama Bank (GBB) which are separated by the North-west Providence  
105 Channel (Fig. 1).

106 The Little Bahama Bank is the second largest isolated platform in the Bahamas and is located in the  
107 northernmost part of the archipelago (Fig. 1). The north-western side of the slope is characterized by the  
108 ‘Little Bahama Bank drift’, a modern periplatform drift, mainly supplied by off-bank sediment transport  
109 from the near-by carbonate platform (Chabaud *et al.*, 2016). The development of such carbonate drift in  
110 this particular location results from the combined action of currents and sediment supply (Mullins *et al.*,  
111 1980; Betzler *et al.*, 2014; Tournadour *et al.*, 2015; Chabaud *et al.*, 2016). The north-eastern slope of the  
112 Little Bahama Bank is incised by two 163 km and 56 km long carbonate canyons, the Great Abaco Canyon  
113 (GAC) and the Little Abaco Canyon (LAC; Mulder *et al.*, 2018), respectively, with their mouths opening to  
114 the Blake Basin and extending to the toe of the Blake Bahama Escarpment at 5000 m water depth (Fig. 2).

115 The physiography, sediment transport and deposition processes of the Bahamian carbonate platforms  
116 also depend on ocean circulation and currents. In particular, two main currents affect the Little Bahama  
117 Bank (Fig. 1): the Antilles Current and the Florida Current. The Antilles Current flows northward along the  
118 eastern side of the LBB and is composed of water coming from the south (Fig. 1). To the west of the LBB,  
119 the Florida Current also flows northward and is formed by waters from both the Caribbean Sea and the  
120 Gulf of Mexico. North of the Little Bahama Bank, at the exit of the Florida Strait, these two currents merge  
121 to form the Gulf Stream (Fig. 1; Neumann & Pierson, 1966; Richardson, 1977). The Deep Western

122 Boundary Current (DWBC; Fig. 1) is a deep current (1000 to 5000 m deep) flowing southward along the  
123 BBE at about 70 cm/s (Hollister & Heezen, 1972). It corresponds to the deepest part of the North Atlantic  
124 Deep Water (NADW; Meinen *et al.*, 2004). Fauquembergue (2018) suggested that another current, the  
125 Antarctic Bottom Water (AABW; Fig. 1) might have impacted the deeper part (>4800 m) of the study area  
126 in the past, especially during glacial periods.

## 127 **Climate**

128 The climate in the Bahamas archipelago is tropical and bi-seasonal. Precipitation is abundant during  
129 summer, while winters are dry, and the annual temperature average *ca* 25°C. The mean annual rainfall is  
130 857 mm and increases northward (Buchan, 2000). Hurricanes hit the archipelago from August to October  
131 three times every four years on average (Buchan, 2000), and on average over the year, cold fronts affect it  
132 23 times (Hardy & Henderson, 2003).

## 133 **Geological context**

134 The present day physiography of the Bahamas resulted from successive tectonic phases initiated by  
135 Pangaea dislocation during the Jurassic (Duncan & Hargraves, 1984; Engebretson *et al.*, 1985; Ross &  
136 Scotese, 1988; Pindell, 1994; Meschede & Frisch, 1998; Coates *et al.*, 2004; James, 2009). The Bahamas  
137 giant carbonate platform initiation began during Late Jurassic rifting with accumulation of shallow marine  
138 deposits and evaporites until the Early Cretaceous (Austin *et al.*, 1986; Sheridan *et al.*, 1988). This giant  
139 platform extended from the Blake Plateau to the Blake Bahama Escarpment where a reef system developed  
140 (Sheridan *et al.*, 1988) and allowed the development of the Little Bahama Bank (Sheridan & Osburn, 1975;  
141 Austin *et al.*, 1986; Sheridan *et al.*, 1988). The Atlantic crust was affected by fracture zones due to rifting  
142 activity associated to the Pangaea Dislocation. In particular, regional magnetic data reveals the presence of  
143 the Bahama Fracture zone or Great Abaco Fracture zone which affects the northern sector of the Bahamas  
144 (Fig. 1; Sheridan & Osburn, 1975; Benson *et al.*, 1978; Mullins *et al.*, 1982).

## 145 **Sediment exports**

146 Part of the offshore material exported from the platform is transported through dense hyperpycnal water  
147 sinking in the ocean (Wilson & Roberts, 1995). This process, called density cascading, is very efficient and  
148 some high-density cascading events are able to transport coarse-grained sediment to the slope (Wilson &  
149 Roberts, 1995). Density cascading is strongly controlled by seasonal changes. In summer, heat and  
150 moisture are parameters controlling processes such as evaporation, which can cause a slight increase in  
151 salinity and therefore can trigger density-driven flows (Wilson & Roberts, 1992, 1995). In winter, cold  
152 fronts generate density disequilibrium between the shallow platform and ocean surface waters. Surface

153 waters are cooled by the cold front, enhancing evaporation and increasing salinity, and ultimately leading to  
154 the sinking of dense post-cold front platform waters (Wilson and Roberts, 1992, 1995). During cold front  
155 events, the fine-grained, bank-derived material is exported by density cascading and deposited on the  
156 uppermost slope, forming the Holocene wedge (Fauquembergue *et al.*, 2018).

157 During periods of major flooding of the Little Bahama Bank corresponding to sea-level highstands in  
158 the Late Pleistocene, off-bank transport was the main transport process from the carbonate bank to the  
159 slope ( Hine & Neumann, 1977; Hine *et al.*, 1981; Chabaud *et al.*, 2016). The ‘spin circle’, a circular flow  
160 pattern induced by ebb and flood currents around shoals, promotes the accumulation of ooids in tidal deltas  
161 (Reeder & Rankey, 2009; Mulder *et al.*, 2017). Only fine-grained mud can be partially exported through  
162 the ebb-flood sediment transport (tidal flushing) that occurs predominantly after storms (Mulder *et al.*,  
163 2017). This sediment flushing supports off-bank transport: the fine bank-derived fraction, when mixing  
164 with pelagic production, leads to the formation of the periplatform ooze on the uppermost slope (Chabaud  
165 *et al.*, 2016). Pelagic sedimentation is the predominant process at play in the study area, while the  
166 deposition of off-bank material is concentrated in the Little Bahama Bank drift (Fauquembergue, 2018).

## 167 **DATA AND METHODS**

168 The Carambar project aims at understanding the sediment transfer between the platform and the deep basin  
169 in a terrigenous-free carbonate environment. Leg 2 of the Carambar cruise (Fig. 1; November 2010 on the  
170 *R/V Le Suroît*) was dedicated to the study of the north-west slope of the Little Bahama Bank (Fig. 1;  
171 Tournadour *et al.*, 2015, 2017a; Chabaud *et al.*, 2016). Carambar 1.5 cruise (November 2014 on the *R/V*  
172 *F.G. Walton Smith*) focused on the uppermost slope of the LBB (Fig. 1; Mulder *et al.*, 2012a). The north-  
173 eastern sector of the Little Bahama Bank slope and the abyssal plain, including the Great Abaco Canyon  
174 and Little Abaco Canyon, were studied during Leg 1 of the Carambar 2 cruise (December 2016 on the *R/V*  
175 *L’Atalante*; Fig. 1; Mulder *et al.*, 2018). Bathymetric and backscatter data from a Kongsberg EM302  
176 (Carambar) (Kongsberg Group, Kongsberg, Norway), a Teledyne Reson Seabat 7125 (Carambar 1.5)  
177 (Teledyne Technologies Inc., Thousand Oaks, CA, USA) and a Kongsberg EM122/EM710 (Carambar 2),  
178 as well as Very High Resolution (VHR) (Chirp) and high resolution seismic data from four air guns and a  
179 192-channel streamer were acquired simultaneously during each cruise covering more than 24 650 km<sup>2</sup>  
180 (Fig. 1). The multibeam echo-sounders are characterized by a transmission frequency operating between 50  
181 m and 12 000 m depth. This allows the simultaneous acquisition of: (i) bathymetric data based on the  
182 calculation of the round-trip time of the emitted acoustic waves; and (ii) acoustic reflectivity, a function of  
183 the intensity of the backscattered signal dependent on the lithology of superficial sediments (i.e. nature and  
184 induration/lithification). The bathymetric data were cleaned of aberrant probes with the CARAIBES  
185 software (©Ifremer) and the reflectivity data were compensated for signal directivity with the SonarScope

186 software (©Ifremer, Augustin & Lurton, 2005). These data were then gridded to obtain bathymetric and  
187 acoustic reflectivity maps with a spatial resolution of 25 m (Carambar 1 and Carambar 1.5) to 50 m  
188 (Carambar 2).

189 Gravity cores with a length ranging between 1 to 11 m were also recovered with a Kullenberg  
190 coring system. During the three cruises, the ‘Chirp’ sub-bottom profiler provided more than 5496 km of  
191 VHR seismic profiles penetrating up to 60 to 80 ms two-way travel time. The definition of seismic facies  
192 was based on these datasets, using backscatter, geometry, amplitude and continuity of the seismic  
193 reflections to establish a facies classification. To facilitate the exploitation of this large dataset,  
194 morphological and sedimentological structures were defined according to a backscatter classification based  
195 on acoustic facies and a VHR seismic classification based on echofacies.

196 Changes in backscatter values correspond to variations in nature, texture and state of the sediments  
197 and/or the sea-bed morphology (Hanquiez *et al.*, 2007, 2010; Principaud *et al.*, 2018) while the VHR  
198 seismic profiles reveal(s) subsurface geometry characteristics and small-scale morphology (for example,  
199 seafloor rugosity). For the acoustic facies, the categories are based on the amplitude of the reflectivity and  
200 on the patterns observed. For the echofacies, the categories are based on the amplitude and geometry of the  
201 reflectors. These classifications provide information regarding seafloor and subsurface sedimentological  
202 parameters. Studies in siliciclastic (Damuth & Hayes, 1977; Damuth, 1980; Hanquiez *et al.*, 2007, 2010)  
203 and carbonate environments (Mullins & Neumann, 1979; Mullins *et al.*, 1984; Tournadour, 2015;  
204 Principaud *et al.*, 2018) linking echofacies and lithology provide a basis for interpreting these echofacies in  
205 terms of depositional environments and allows for calibration of interpretations. The association of acoustic  
206 facies, echofacies and morphobathymetry were integrated in a general classification of sedimentary facies  
207 (Table 1). Various spatial analyses and maps were produced using ArcGIS for Desktop software (©Esri).

## 208 **RESULTS**

### 209 **Little Bahama Bank slope, Great Abaco Canyon and Little Abaco Canyon morphology**

210 The north slope of the Little Bahama Bank can be subdivided in four parts according to slope morphology  
211 (Fig. 2A to C). These subdivisions are based on previous work (Rankey & Doolittle, 2012; Tournadour,  
212 2015) and redefined considering the new bathymetric data provided by the Carambar 2 cruise which  
213 evidence a steeper slope than the previous domains. These redefined subdivisions were introduced to assure  
214 the homogeneity and logical continuity of domains from the eastern and western sectors of the study area  
215 (Fig. 2C). The adapted domains reflect the morphology of both the western and eastern sides of the Little  
216 Bahama Bank slope.

217 **1** The uppermost slope extends from the platform edge to 240 to 300 m water depth. It is relatively  
218 smooth, constitutes the steepest ( $>15^\circ$ ) slope of the LBB and includes a sediment wedge (Fig. 2A to C;  
219 Mulder *et al.*, 2012b; Fauquembergue *et al.*, 2018). This wedge can reach up to 35 m in thickness, is mainly  
220 Holocene in age and is separated from the platform by four 10 to 20 m deep and 50 km wide terraces  
221 (Mulder *et al.*, 2012b; Fauquembergue *et al.*, 2018).

222 **2** The upper slope extends from 240 to 300 m to 650 m water depth. It has a gradient of 1 to  $2^\circ$  and is  
223 incised by slope canyons (Fig. 2A to C). Only the linear part of these canyons is included in this slope  
224 sector. A mass transport complex (MTC) was described by Tournadour *et al.* (2015) in its westernmost part  
225 (Fig. 2).

226 **3** The middle slope extends from 650 to 1000 m water depth and its gradient increases from  $1^\circ$  in the west  
227 to 3 to  $4^\circ$  in the east (Fig. 2A to C). This slope is incised by the slope canyon (Fig. 3A). Bathymetric highs  
228 followed by depressions represent slide scars. They affect the part of the slope situated between the  
229 canyons all along the slope. Other structures such as carbonate mounds and pockmarks are situated in the  
230 western part of the middle slope (Fig. 3B).

231 **4** The lower slope extends from 1000 to 1500 m water depth with a gradient increasing towards the  
232 abyssal plain from 0.6 to  $4^\circ$  (Fig. 2A to C). In this part of the slope, several structures can be observed. 1 to  
233 20 m deep straight, parallel furrows affect the seafloor mostly in the west (Fig. 4A). Other erosional 1 to 10  
234 m deep furrows oriented N300 to N270 cross-cut the former furrows and extend eastward (Fig. 4A). Both  
235 types of furrows extend over several kilometres and are spaced hundreds of metres apart. Undulated  
236 structures with a 5 m amplitude can be observed on the seafloor upstream of the Little Abaco Canyon (Fig.  
237 4B). In the northern part of the study area, the Blake Plateau dips towards the east with a gradient of  $0.5^\circ$   
238 between *ca* 1200 to 1600 m water depths. Mass movements, which are evidenced by scars ('S'; Fig. 4C),  
239 gullies and a valley leading to the Great Abaco Canyon also dissect this plateau.

240 The Great Abaco Canyon and Little Abaco Canyon are U-shaped (with a length of 163 km and 56 km  
241 respectively; Fig. 5A). These two canyons are punctuated by knickpoints and oversized chutes (Fig. 5C and  
242 D). These chutes are over 500 m high and are followed by 279 m, 113 m (LAC), 150 m, 140 m and 113 m  
243 (GAC) depressions called plunge pools (Figs 5A, 5B, 6A and 6B; Mulder *et al.*, 2018). The GAC and LAC  
244 are parallel to the LBB edge and are aligned with the Great Abaco Fracture Zone (GAFZ), whereas the  
245 upper and middle slope of the LBB are affected by canyon incisions which are perpendicular to the margin.  
246 South of the Great Abaco Canyon, a relict plateau situated at 1000 m water depth displays evidences of  
247 mass movement ('S'; Fig. 4C) and is incised by two valleys. Twenty kilometres away from the Great



248 Abaco Canyon and 7 km south of the Little Abaco Canyon, two 5 km long canyons incise the Blake  
249 Plateau and the slope through the Blake Bahama Escarpment, respectively (Fig. 2A).

250 The south-east limit of the plateau consists of the SSW–NNE oriented Blake Bahama Escarpment  
251 (Fig. 2). This feature is a 2000 m high and 60° steep escarpment. It separates the Blake Plateau from the  
252 Atlantic Abyssal Plain lying at 4900 m water depth. The bathymetry shows 50 km long chaotic deposits  
253 extending over 20 km away from the escarpment [mass wasting deposits (MWD); Fig. 2A]. A more than  
254 200 m thick sediment bulge extends at the mouth of the Great Abaco Canyon in the abyssal plain.

### 255 *Acoustic facies*

256 The identification of acoustic facies is based on the intensity of the backscatter and the patterns of  
257 reflections observed inside (Fig. 7). In this work, the darkest colours correspond to high-reflectivity  
258 (implying either coarse sediments, indurated sediments or both) and lighter colours correspond to low  
259 reflectivity (finer and softer sediments). In the study area, backscatter tones can be subdivided into eight  
260 categories (Table 2; Fig. 8).

261 **1** The very high-reflectivity homogeneous acoustic facies is observed only in few parts of the study area.  
262 This the acoustic facies is found: (i) at the toe of the Blake Bahama Escarpment; (ii) in the 5 km long  
263 canyon in the northern sector of the Great Abaco Canyon; (iii) in the steepest part of the Great Abaco  
264 Canyon; and (iv) in the flanks of the Little Abaco Canyon (Fig. 8). In the western sector of the study area,  
265 this facies makes up: (i) the uppermost slope; (ii) the area upstream from the small canyons; as well as (iii)  
266 the edge of the scars between canyons.

267 **2** The very high-reflectivity heterogeneous acoustic facies (Table 2) is characterized by alternation of  
268 very-high reflectivity and patches of high reflectivity. It is associated with the main part of the flank of the  
269 Blake Bahama Escarpment and both sides of the Great Abaco Canyon (Fig. 8).

270 **3** The high-reflectivity homogeneous acoustic facies covers a large part of the upper slope and proximal  
271 part of the abyssal plain (Fig. 8). It was evidenced between the canyons that incise the western part of the  
272 upper slope, and in the MTC structure on the eastern sector as well as on the Blake Plateau. This facies also  
273 corresponds to a part of the flank of the Blake Bahama Escarpment and the deposits contiguous to the  
274 Blake Bahama Escarpment between the Little Abaco Canyon and the Great Abaco Canyon and north of the  
275 Great Abaco Canyon, in the deep basin. It also covers the 5 km long canyon south of Little Abaco Canyon.

276 **4** The high-reflectivity heterogeneous acoustic facies corresponds to high-reflectivity with medium  
277 reflectivity lineations of two types: (i) lineations extending from the canyons in the western part of the  
278 slope and the valley feeding the giant canyons; and (ii) N300 to N270 oriented lineations in the eastern

279 Little Bahama Bank lower slope (Tournadour, 2015). This area also covers a part of the relict plateau  
280 between the Great Abaco Canyon and the Little Abaco Canyon (Fig. 8).

281 **5** The medium homogeneous reflectivity acoustic facies is the most frequent acoustic facies encountered  
282 in the study area. It covers the abyssal plain, the canyons incising the upper slope, the smooth parts of the  
283 middle slope and the western part of the study area including the smooth parts of the Blake Plateau at the  
284 lower slope.

285 **6** The medium patchy heterogeneous reflectivity acoustic facies corresponds to medium reflectivity with  
286 patches of high reflectivity. It is present at the transitions between high acoustic facies and medium  
287 acoustic facies in the lower slope (Fig. 8).

288 **7** The medium undulated heterogeneous reflectivity acoustic facies is characterized by medium reflectivity  
289 with high-reflectivity undulated structures. It is mostly present in the western part of the slope and  
290 corresponds to the transition between the furrows of different slope canyons (Fig. 8).

291 **8** The medium punctuated heterogeneous reflectivity acoustic facies is characterized by medium  
292 reflectivity with small circular patches of high reflectivity with a diameter of 100 to 200 m. It covers a large  
293 part of the relict plateau between the Great Abaco Canyon and the Little Abaco Canyon, areas at the end of  
294 the furrows in the western part of the study area and some parts of the Blake Plateau (Fig. 8).

295

## 296 *Echofacies mapping*

297 The VHR seismic mapping was realized using an echofacies classification based on the amplitude and the  
298 geometry of the seismic signal (Table 3). Five echofacies can be defined in the study area (Table 3; Fig. 9).

299 **1** The bedded echofacies covers the majority of the western part of the upper slope (unaffected by  
300 canyons), the uppermost slope wedge, the sediment over the MTC, the part without slides of the Blake  
301 Plateau and the northern part of the deep basin, at the mouth of the Great Abaco Canyon (Fig. 9). It is  
302 found predominantly in areas with a gentle slope ( $\leq 1$ ).

303 **2** The hyperbolic echofacies occurs where the slope is steeper, when the slope abruptly changes, in the  
304 canyons incising the upper slope, in the Great Abaco Canyon and Little Abaco Canyon, in the 5 km long  
305 canyons C1 and C2 (Figs 2 and 9), and on the Blake Bahama Escarpment and its associated deposits (Fig.  
306 9).

307 **3** The blind echofacies is the least developed of the facies. It corresponds to the shallower part of the  
308 uppermost slope of the study area and appears sparsely in the Blake Bahama Escarpment and on plane  
309 surfaces of the Blake Plateau. It also covers the smooth areas separating the furrows on the western lower  
310 slope.

311 **4** The combined I (hyperbolic + blind) echofacies corresponds to slightly diffuse bedded reflections with  
312 hyperboles. This facies covers two major parts of the study area: (i) the southern part of the basin at the  
313 mouth of the Little Abaco Canyon; and (ii) the western part of the study area in the lower slope  
314 corresponding to the mouths of the slope canyons (Fig. 9). This last part overlaps the furrows and the N300  
315 lineations affecting the seafloor. Combined I echofacies covers an important part of the head of the Great  
316 Abaco Canyon. It also appears more locally upstream of failure scars that cover part of the Blake Plateau.

317 **5** The combined II (hyperbolic + bedded) echofacies corresponds to bedded reflections overlying the  
318 hyperboles. It appears mainly in the tributaries feeding the Great Abaco Canyon and the Little Abaco  
319 Canyon as well as on the flanks of the Great Abaco Canyon (Fig. 9). This echofacies is also present in the  
320 canyons of the east upper slope, in patches on the Blake Plateau, in the mass wasting deposits and in the  
321 eastern part of the basin.

322 The combined study of bathymetry, acoustic facies and echofacies compared with previous studies  
323 (Hanquiez *et al.*, 2007, 2010; Tournadour, 2015; Principaud *et al.*, 2018) allowed for the definition for  
324 different domains, which are each associated with different processes (Table 1; Figs 10, 11 and 12A).

## 325 **INTERPRETATIONS AND DISCUSSION**

### 326 **Sedimentary processes along the northern Little Bahama Bank slope**

#### 327 *Depositional processes*

#### 328 *Hemipelagic and contouritic deposits.*

329 In the western part of the study area, the slope is characterized by overall homogeneous, medium  
330 reflectivity acoustic facies and bedded echofacies. This facies corresponds to deposits linked to the export  
331 of carbonate mud from the platform (facies 1, Figs 11 and 12B; Tournadour *et al.*, 2015), as well as  
332 contourite deposits which characterize the Little Bahama Bank drift (Chabaud, 2016). Both hemipelagic  
333 and contouritic deposits are susceptible of producing this facies as they promote the deposition of fine-  
334 grained sediment (medium homogeneous reflectivity) with low impedance contrast (bedded echofacies).  
335 Furthermore, the size scale of the LBB drift is such that its geometries are not visible at the resolution of  
336 this study. The presence of such acoustic facies over the MTC suggests that it is covered by a hemipelagic

337 blanket. This mainly medium homogeneous reflectivity zone with smaller medium heterogeneous patchy  
338 reflectivity facies zone are associated with hyperbolic echofacies. The hyperboles are likely related to the  
339 steep edges of the dome shape geometry and thus highlight the presence of deep-water carbonate mounds  
340 (facies 2, Fig. 11; Tournadour *et al.*, 2015).

341 This facies association also appears in other regions of the study area like the Blake Plateau or the  
342 plateau situated between the Little Abaco Canyon and the Great Abaco Canyon (Fig. 11). It corresponds to  
343 flat areas suggesting hemipelagic sedimentation (facies 1, Fig. 11).

#### 344 *Periplatform ooze.*

345 The uppermost slope is characterized by blind echofacies, followed downslope by bedded echofacies  
346 associated with medium reflectivity which correspond to a Holocene sediment wedge and the terraces  
347 overhanging it (Figs 8 and 9; Rankey & Doolittle, 2012). The homogeneous and medium homogeneous  
348 nature of the reflectivity in this area suggests the presence of soft, fine-grained, bank-derived sediment  
349 mixed with pelagic production. The presence of these acoustic facies and the bedded echofacies is  
350 consistent with periplatform ooze deposits in the uppermost slope (facies 3, Fig. 11). Echofacies located on  
351 the uppermost and upper slope correspond to bank-derived sediments, while bedded echofacies located on  
352 the northern Blake Plateau correspond to contouritic and pelagic blankets (Fauquembergue, 2018).

#### 353 *Turbiditic deposits.*

354 A *ca* 3 km large circular-shaped structure, represented by combined blind and hyperbolic echofacies and  
355 homogeneous medium-reflectivity acoustic facies, can be observed in the eastern part of the lower slope, in  
356 the downslope extension of the canyons (Fig. 4B). The analysis of a sediment core located in this feature  
357 revealed coarse-grained sediments with a relatively high sedimentation rate (12 cm/kyr; Fauquembergue,  
358 2018). It is suggested in this study that this structure corresponds to a lobe deposited at the mouth of a 10  
359 km long canyon (Fig. 4B). In addition, 5 m amplitude structures extending over 4 km over this lobe can be  
360 interpreted as sediment waves (Fig.4B). Here, sediment waves refer to a generic term to describe undulated  
361 features since the resolution does not provide any further information regarding their nature (dunes, cyclic  
362 steps, etc). This lobe fills a small depression and its volume can be estimated to  $240 \times 10^6 \text{ m}^3$   
363 (Fauquembergue, 2018). It implies recent activity of sediment transport through the slope canyon to the  
364 head of the Little Abaco Canyon and highlights the modern activity of the eastern slope canyons. It also  
365 suggests turbidity flows and export activity upstream of the Little Abaco Canyon (facies 4, Fig. 11).

#### 366 *Base of slope deposits.*

367 On the lower slope of the western part of the study area (Fig. 11), downstream of the canyons and furrows,  
368 medium reflectivity punctuated facies is associated with bedded and blind echofacies and displays a fan-

369 shaped structure. The association of both medium reflectivity and bedded echofacies implies that sediment  
370 dynamics are dominated by depositional processes. The presence of high amplitude reflectors which overlie  
371 diffuse reflectors associated with higher reflectivity suggests the presence of more indurated or coarser-  
372 grained sediments than the hemipelagic blanket observed westerly. Therefore, this association also suggests  
373 low deposition rates and/or slight induration of those grainy deposits (facies 5, Fig. 11).

#### 374 *Mass wasting deposits.*

375 On the Blake Bahama escarpment and 20 km eastward in the basin, hyperbolic echofacies and  
376 homogeneous, very high to high reflectivity acoustic facies co-occur with 50 km long chaotic deposits  
377 extending over the escarpment. These chaotic deposits were interpreted as mass wasting deposits  
378 originating from stacking events of the mass movement of hundreds of metres thick sediments from the  
379 Blake Bahama Escarpment (Mulder *et al.*, 2018). The high reflectivity and hyperbolic echofacies suggests  
380 that the chaotic deposits are indurated and coarse-grained, probably blocky, and of considerably large size  
381 (facies 6, Figs 11 and 12B). These deposits could correspond to calciturbidites or calcidebrites as observed  
382 in Exuma Sound (Reijmer *et al.*, 2012). The hyperbolic echofacies suggests that these deposits accumulated  
383 with steep edges or contain blocks of consequent size. These chaotic deposits are separated on both sides of  
384 the Great Abaco Canyon by a large band of bedded echofacies associated with homogeneous, medium-  
385 reflectivity (Figs 8 and 9).

386 At the mouth of the Little Abaco Canyon, the hyperbolic facies is associated with homogeneous  
387 and heterogeneous high-reflectivity acoustic facies extending 8 km away from the canyon. This facies  
388 association suggests that hard and/or coarse-grained sediments form the lobe at the mouth of the Little  
389 Abaco Canyon (Fig. 4D).

390 Mass wasting events originating from the Blake Bahama Escarpment likely accounted for a significant  
391 portion of the sediment supply towards the basin. Conversely, the Great Abaco Canyon likely contributed  
392 to a minor extent as a sediment source, since no erosion or depositional (lobe) structures were evidenced by  
393 bathymetric survey at its mouth. At the mouth of the Little Abaco Canyon, four 50 to 100 m high  
394 knickpoints can be observed within the mass wasting deposits. This suggests recent or important canyon  
395 activity resulting in the formation of supercritical flows which lead to the development of hydraulic jumps  
396 (Komar, 1971). In turn, these hydraulic jumps produce knickpoints and, ultimately, contribute to  
397 maintaining the fresh appearance of the knickpoints (Guiastrennec-Faugas *et al.*, 2020).

#### 398 *Abyssal plain deposits.*

399 Homogeneous medium reflectivity acoustic facies cover the Blake Bahama abyssal plain and are associated  
400 with bedded echofacies in the north or combined I reflectivity in the south. This implies that they are made

401 up of fine-grained or slightly indurated sediments (facies 7, Fig. 11). Regardless of sediment nature, VHR  
402 seismic data shows thin-bedded reflections over a high amplitude reflection that could correspond to  
403 basaltic oceanic crust, suggesting a thin sediment cover.

#### 404 *Erosion and bypass processes*

##### 405 *Hardgrounds.*

406 The western part of the upper slope and the central part of the middle slope are characterized by  
407 homogeneous high-reflectivity acoustic facies separated by strips of homogeneous medium reflectivity.  
408 These facies are respectively associated with bedded and hyperbolic echofacies and are likely connected to  
409 the numerous 2 to 20 km long canyons and the inter-canyon plateaus (facies 8 and 9, Fig.11). The presence  
410 of the hyperbolic facies is consistent with the abrupt change of slope gradient on the canyon edge walls and  
411 the reflection of the acoustic signal. The homogeneous high-reflectivity acoustic facies combined with the  
412 bedded echofacies is restricted to the smooth part of the inter-canyon slope. The high-reflectivity acoustic  
413 facies indicates low penetration of the acoustic signal in the sediments in this area and are consistent with  
414 the high-amplitude bedded reflections. This could imply early cementation (facies 10, Fig. 11). The  
415 analysis of core CARKS26, located at the base of the middle slope (Fig. 2A), shows periplatform ooze  
416 deposits containing indurated nodules corresponding to a facies described by Tournadour (2015) and  
417 Chabaud (2016) as the nodular ooze facies (facies 9, Fig. 11). It suggests an induration gradient  
418 (Tournadour *et al.*, 2017) and bypass transport along the smoothest part of the slope, reflected by an  
419 increase in reflectivity intensity down the slope.

420 Between 78°24'W and 77°21'W, the lower slope shows an irregular surface characterized by a  
421 heterogeneous, high-reflectivity acoustic facies with medium reflectivity lineations (Fig. 8) associated with  
422 a combination of bedded, blind and hyperbolic echofacies. This area displays furrows extending from the  
423 canyons, eroding the slope and finally gently bending eastward (Figs 2A and 4A) in the slope direction.  
424 Both high reflectivity and the blind part of the echofacies suggest an induration of this part of slope that  
425 could be related to the presence of furrows (facies 10, Figs 11 and 12B). This suggests down-slope  
426 gravitational processes (facies 10, Figs 11 and 12B). These structures are cross-cut by perpendicular  
427 erosional furrows, oriented N300 to N270 (Fig. 4A) that are interpreted as the results of the action of either  
428 the northward flowing Antilles Current or the southward flowing Labrador Current (upper part of the  
429 DWBC). These furrows related to medium reflectivity lineation are responsible for the hyperbolic  
430 component of the combined echofacies.

431 *Failure scars.*

432 The cover of the MTC present in the western sector of the study area is associated with homogeneous,  
433 medium-reflectivity acoustic facies and bedded echofacies while its edge is composed of homogeneous  
434 very high-reflectivity facies (facies 12, Fig. 11). The very high-reflectivity facies is likely related to the  
435 steep and indurated walls of the MTC.

436 The lower slope of the Blake Plateau corresponds mainly to bedded, hyperbolic and combined  
437 echofacies linked respectively with homogeneous medium-reflectivity or high-reflectivity and  
438 heterogeneous medium-reflectivity facies. No slump scars were evidenced in the large flat area of the  
439 contouritic plateau suggesting that it is not affected by mass movement and is covered with bedded  
440 echofacies and homogeneous medium reflectivity acoustic facies. This suggests a lesser induration  
441 (Hanquiez *et al.*, 2007, 2010; Principaud *et al.*, 2018) of the sediment (facies 1, Fig. 11). These scars that  
442 affect the contouritic Blake Plateau can be related to sliding motion (facies 11, Fig. 11). The scars cause  
443 heterogeneities in reflectivity and are responsible for the variety of the combined facies which is expressed  
444 in reliefs and hyperbolae generated by failure scars in a generally bedded system. In addition, the high-  
445 reflectivity of these facies suggests a higher state of induration, especially on the slide edges. The high-  
446 reflectivity lineations in this zone are similar to the N300 to N270 lineations. High-reflectivity affects the  
447 edge of the Blake Plateau, suggesting erosion and/or bypass by bottom currents (DWBC or Antilles  
448 Current).

449 Based on bathymetry, Mulder *et al.* (2018) proposed that slide scars observed on the southern side  
450 of the relict plateau might be circumstantial evidence of a lateral supply of sediment to the Little Abaco and  
451 the Great Abaco Canyons. This study's results are consistent with these observations, as heterogeneous,  
452 medium-reflectivity facies with medium reflectivity patches are associated with bedded echofacies  
453 corresponding to flat areas. This association suggests hemipelagic sedimentation with no movements  
454 (facies 1, Fig.11). On the contrary, combined and hyperbolic echofacies are associated with high-  
455 reflectivity heterogeneities oriented towards the Little Abaco and Great Abaco Canyons. These facies  
456 correspond to a relict contouritic plateau affected by numerous slides inducing a downslope sediment  
457 motion towards both the Little Abaco Canyon and the Great Abaco Canyon (facies 11 and 13, Figs 11 and  
458 12B).

459 Heterogeneous, medium-reflectivity acoustic facies are associated with hyperbolic echofacies and  
460 abrupt changes in the slope upstream of the Little Abaco Canyon. The hyperbolic echofacies is related to  
461 intense sliding in this area, while the high reflectivity suggests coarse-grained or more indurated deposits.  
462 The volume of sediment originated from slides appears to be more important at the toe of the northern flank  
463 of the Great Abaco Canyon than on its southern flank, suggesting that the sliding source comes

464 preferentially from the Blake Plateau located north of the Great Abaco Canyon (Fig. 12B). A strip of  
465 combined (bedded and hyperbolic) echofacies and heterogeneous, medium-reflectivity acoustic facies, in  
466 the south of the Little Abaco Canyon, likely corresponds to a terrace and suggests less indurated sediments  
467 (since the bedded part of the facies indicates deposition processes).

468 *Slope canyons.*

469 In the eastern part of the slope, the spacing between slope canyons of the same size scale is less regular.  
470 This part of the slope is affected by mass movements and scars that could evidence sliding (Fig. 13A). The  
471 canyons correspond to medium homogeneous reflectivity facies associated with combined hyperbolic  
472 echofacies due to the reflection of the acoustic signal on the steep canyon edge walls (facies 8, Fig. 11).

473 The eastern inter-canyon slope is associated with high homogeneous reflectivity, which suggests  
474 early cementation as in the western part of the slope (facies 9, Fig. 11). The smooth part of the inter-canyon  
475 plateaus, as observed on the western part of the study area, is represented by bedded and combined I  
476 (hyperbolic + bedded) echofacies. The hyperboles observed are due to the steep walls of the slide scars  
477 affecting the canyons and inter-canyon parts of the slope.

478 The association of heterogeneous high-reflectivity acoustic facies with combined I echofacies and  
479 erosive lineations characterizes the valley feeding the head of the Great Abaco Canyon. These facies  
480 suggest that the sediments covering the seafloor of the Great Abaco Canyon head are indurated or coarse-  
481 grained (facies 10, Figs 11 and 12B). The narrow head and the erosion structures suggest that the canyon  
482 head does not represent the main source of modern sediments settling in the canyon. The two other  
483 tributaries draining the south-eastern part of the slope are characterized by a combined II echofacies and  
484 homogeneous medium reflectivity, suggesting less-indurated deposits and a depositional tendency (facies  
485 13, Figs 11 and 12B). The Great Abaco Canyon flanks and floor are associated with combined and  
486 hyperbolic echofacies as well as patches of medium to very-high reflectivity. This suggests the existence of  
487 both erosional and depositional processes in the canyons. It also suggests that mass movements affect the  
488 canyon edges and contribute to supplying downslope transport processes (Fig. 12B). This observation is  
489 consistent with the presence of terraces interpreted as originating from slumped masses in canyon-head  
490 amphitheatres (Mulder *et al.*, 2018)

491 The two 5 km long canyon (C1 and C2) bodies and mouths incising the Blake Plateau and crossing the  
492 BBE are covered with hyperbolic echofacies associated with very-high reflectivity and high-reflectivity  
493 facies (facies 14, Fig. 11). This suggests the presence of indurated deposits and implies that the sediments  
494 transiting through them do not accumulate at the mouths of these canyons.



495

## 496 **Sediment distribution and transport along the Little Bahama Bank slope**

497 Sediment export along the Little Bahama Bank slope is strongly controlled by the morphology of the  
498 platform and the related hydrodynamic processes. This results in a complex distribution of sediments.

### 499 *Difference between the eastern and western sectors of the LBB slope*

500 In the western sector of the LBB, the deposition of fan-shaped deposits are due to sediment flows forming  
501 furrows (Tournadour *et al.*, 2017) and spreading out at the base of the slope (facies 5, Fig. 11). Different  
502 processes seem to occur in the eastern sector of the LBB. Distributary furrows extend from the eastward  
503 canyons situated between Bahama Bay and Spanish Cay (Fig. 12B) but fan-shaped base of slope deposits  
504 do not exist at their mouth (Fig. 12B). The presence of sediment waves and lobate structures (facies 4, Fig.  
505 11) filled with coarse-grained material suggests that turbiditic flows transit through the eastern canyons. On  
506 the contrary, those transiting troughs the western canyons terminate in relatively finer-grained deposits  
507 (facies 5, Fig 11). Thus, it is interpreted that low-density flows cut across the western canyons while  
508 relatively higher density flows go through the eastern canyons (Fig. 12B).

509 In addition, the presence of medium homogeneous reflectivity facies at the toe of the eastern  
510 canyons is generally indicative of less-indurated sediment than in the western part of the LBB which  
511 displays medium reflectivity facies punctuated with high reflectivity zones (Fig. 8). These spatial  
512 disparities in the acoustic facies implies different activity of the eastern *versus* western canyons.  
513 Accordingly, the presence/absence of hemipelagic deposits and base of slope deposits are reliable criteria  
514 which delimited the western and eastern part of the Little Bahama Bank slope (Fig. 12B).

### 515 *Sediment transit through Little Abaco and Great Abaco Canyon*

516 The presence of levee-shaped deposits between the two major Great Abaco Canyon tributaries indicate that  
517 dilute turbidity currents supply much of the sediment (Mulder *et al.*, 2018). This is consistent with the  
518 homogeneous medium-reflectivity facies which suggests that sediment deposit and modern active sediment  
519 processes occur in the eastern canyons.

520 Upstream of the head of the Great Abaco Canyon, bypass processes are reflected by high  
521 heterogeneous and combined blind and hyperbolic facies and are associated to a hardground facies (facies  
522 10, Fig. 11). This suggests that sediments pass through the Great Abaco Canyon and are not deposited on  
523 its head. Considering the small size of the canyon head, the small number of slide scars (Fig. 13A) and the

524 low-density currents supplying the western lower slope (Fig. 12B), this suggests less dense sediment supply  
525 transiting from its head (Fig. 12B).

526 Upstream of the Little Abaco Canyon, the acoustic set defining the turbiditic deposits (facies 4,  
527 Table 3) imply that the eastern canyons are highly active. The acoustic set also suggests a direct axial  
528 supply of the Little Abaco Canyon by relatively high-density turbidity currents. It further highlights the  
529 supply difference between the Little Abaco Canyon and the Great Abaco Canyon.

530 North of the study area, 300 km away on the Blake-Bahama Outer Ridge region, erosional furrows  
531 were observed by Hollister *et al.* (1974) at 4 to 5 km water depth and interpreted as the action of contour  
532 current activity. Previously conducted surveys show activity of the DWBC at 26.5°N (Lee *et al.*, 1996;  
533 Bryden *et al.*, 2005; Johns *et al.*, 2005). In addition, the acoustic set associated with the abyssal plain  
534 deposits (facies 7, Fig. 11) suggests slight induration of these deposits. Thus, the DWBC impact on the  
535 material transiting through the canyon mouths cannot be neglected because it could have led to the present-  
536 day absence of topography and visible sediment accumulation at the mouth of the Great Abaco Canyon  
537 (Fig. 12B).

#### 538 *Spatial disparities in sediment processes and canyon maturity along the northern slope of the Little* 539 *Bahama Bank*

540 The difference in the sediment flows transiting through the western *versus* eastern canyons emphasizes the  
541 existence of spatial disparities in deposition processes along the Little Bahama Bank slope (Fig. 14B). The  
542 western sector of northern slope of the LBB generally displays acoustic facies that are indicative of  
543 depositional facies such as hemipelagic deposits (facies 1, Fig. 11), periplatform oozes (facies 3, Fig. 11) or  
544 base of slope deposits (facies 5, Fig. 11). Especially in the westernmost part of the slope, sediment  
545 processes are dominated by almost entirely deposition processes (facies 1, 3 and 5, Fig. 11). On the  
546 contrary, the eastern sector displays more heterogeneous reflectivity facies and combined echofacies (Figs  
547 8 and 9) suggesting the occurrence of erosional and/or bypass processes such as hardgrounds (facies 9 and  
548 10, Fig. 11), slides (facies 11, Fig. 11) and escarpments (facies 13 and 14, Fig. 11), particularly on the  
549 middle slope and the part of the lower slope south of the GAC. Only the easternmost facies (facies 1, Fig.  
550 11) and very localized turbidite deposits (facies 3, Fig. 11) depict the influence of local depositional  
551 processes. This spatial repartition of sediment/deposition processes is also highlighted by the spatial  
552 evolution of the slope canyons. As previously observed on the western part of the LBB slope (Tournadour,  
553 2015; Mulder *et al.*, 2017), a gradient in the maturity of the canyons can be observed between the western  
554 and eastern sectors of the study zone. The morphology of the eastern canyons presenting an amphitheatre  
555 shape (amphitheatre head highlighted by dotted lines in Fig. 13B) and an up dip linear part (Figs 3A and

556 13B) likely corresponds to a mature stage of canyon formation on this slope (Puga-Bernabéu *et al.*, 2011).  
557 Failure scars and more linear canyons can be observed in the central and western sectors and correspond to  
558 the retrogressive phase of the Little Bahama Bank slope canyon formation model. This holistic  
559 investigation of the LBB has enabled the mapping of sediment facies in the area, evidencing spatial  
560 disparities in sediment/depositional processes which ultimately denote an east-west canyon maturity  
561 gradient.

### 562 **Structural influence on Little Bahama Bank slope morphology**

563 While most canyons extend perpendicularly from platform edges, both the Great and Little Abaco canyons  
564 are oriented parallel to the edge of the LBB. The particular direction of these two major canyons coincides  
565 with the Great Abaco Fracture Zone (GAFZ in Fig. 1), suggesting that this structural feature controls  
566 canyons formation and persistence on the LBB slope. The influence of the Great Abaco Fracture Zone  
567 extends over the entire slope of the Little Bahama Bank as evidenced by: (i) the giant canyons which play  
568 an important part in sediment distribution; (ii) a marked east/west difference in platform morphology; and  
569 (iii) an east–west gradient in sediment and deposition processes, as well as a canyon’s maturity. Spatial  
570 disparities in sediment processes were evidenced in this paper in the entire study area, completing previous  
571 observations which focused on the western sector of the LBB slope. The presence of abundant failure scars  
572 and more mature and linear canyons in the eastern sector of the LBB slope indicates that incisions are  
573 concentrated in this sector. This could be the result of slope steepening due to fault motion of the Great  
574 Abaco Fracture Zone. This motion generates differential subsidence between the eastern and western  
575 sectors of the Little Bahama Bank slope, while the edges of the Great Abaco Island define the axis of this  
576 motion. Furthermore, spatial discrepancies in the expression of differential subsidence (i.e. a steeper slope,  
577 sliding motion and the generation of giant canyons in the east, *versus* a gentler slope, and drift and  
578 hemipelagic deposition in the west) is indicative of a weaker direct structural influence in the western part  
579 of the northern Little Bahama Bank slope.

580 Thus, this east/west gradient imply that the inception of differential subsidence was likely linked to the  
581 development of the Great Abaco Fracture Zone. However, further analysis of high-resolution seismic lines  
582 would be necessary to assess the role played by the Great Abaco Fracture Zone in moulding the  
583 morphology of the Little Bahama Bank slope.

### 584 **Little Bahama Bank northern slope morphology and sediment processes: more general implications**

585 The presented multi-tool survey has provided a holistic view of the large (325 km long/24 650 km<sup>2</sup>)  
586 sedimentary system that is the LBB, improving understanding of this system, and allowing a representation  
587 of the complete sedimentary profile from the carbonate shelf edge to the abyssal plain. This work evidences

588 large-scale morphological characteristics and sediment dynamics of an entire carbonate margin from the  
589 shallow upper slope to deeper environments and identified preferential accumulation, bypass and erosion  
590 locations of the carbonate material on the slope. This study's work further highlights the mixed influence of  
591 both pre-existing structural features and sediment dynamics that may occur in a carbonate system such as  
592 the LBB. It provides new lines of investigation with regard to the genesis of giant carbonate canyons. The  
593 results suggest that these systems are structurally generated and moulded over time, with a strong influence  
594 of structural features on 'classic' slope canyon maturity. This has a major impact on carbonate stratigraphic  
595 modelling and carbonate seismo-stratigraphic interpretations in ancient analogue carbonate systems. Future  
596 acquisition of high-resolution seismic profiles in the area may provide further information regarding the  
597 timing of structural effects of the GAFZ on the northern sector of the Bahamas and their implication on the  
598 establishment of the Great Abaco Canyon and the Little Abaco Canyon. Such data covering the entire  
599 northern sector of the Bahamas will provide a complete tectono-stratigraphic framework on which to  
600 reconstruct the genesis of these canyons and define their role in carbonate transport from the slope to the  
601 basin.

## 602 **CONCLUSIONS**

603 The large dataset covering almost the entire northern Little Bahama Bank slope reveals a wide variety of  
604 features attesting to diverse sedimentary processes occurring along the slope and allowing both along-slope  
605 and down-slope transport to supply giant canyons on the windward side of this carbonate margin. Off-bank  
606 transport including tidal flushing and density cascading promote the export of fine-grained and coarse-  
607 grained materials from the platform. This sedimentary load transits through the numerous canyons incising  
608 the middle and lower slope all along the Little Bahama Bank. Prolonging the canyons, distributary furrows  
609 are cross-cut by other furrows evidencing the impact of surface currents and bypass processes on this part  
610 of the lower slope. Despite the moderate sediment supply feeding the Great Abaco Canyon head, the main  
611 supply of this giant canyon appears not to be axial. Many failure scars and slides can be observed in the  
612 eastern part of the lower slope. They affect both the contouritic Blake Plateau, the Little Abaco Canyon and  
613 the Great Abaco Canyon flanks. The downslope motion induced by slides appears to be the main source of  
614 sediment transiting through the canyons. In this way, the two canyons appear to be supplied differently: the  
615 Great Abaco Canyon is mainly laterally supplied, and the Little Abaco Canyon is both axially and laterally  
616 supplied. These dense sediment flows are sufficient to maintain the morphology of the two giant carbonate  
617 canyons. The establishment of these canyons running parallel to the platform was likely related to the Great  
618 Abaco Fracture Zone. Energetic bottom currents (Deep Western Boundary Current and Antarctic Bottom  
619 Water) seem to prevent the present sediment deposition of a lobe at the mouth of the Little Abaco Canyon  
620 and Great Abaco Canyon. The analysis of the backscatter and Very High Resolution seismic data shows a

621 gradient in deposition on the Little Bahama Bank slope. The eastern part of the slope is more subject to  
622 erosion whereas the western part shows more deposition processes. Erosional processes dominate the  
623 eastern part of the slope, while the western part is influenced to a greater extent by depositional processes.  
624 These spatial discrepancies along with the unusual alignment of the giant canyon with the Little Bahama  
625 Bank platform and Great Abaco Fracture Zone suggest that these regions are influenced by a structural  
626 control. The structural control takes root in the regional differential subsidence between the eastern *versus*  
627 western sectors of the Great Abaco Fracture Zone and influences sedimentary dynamics on the slope.

628

## 629 **ACKNOWLEDGEMENTS**

630 We thank the captain and crew of the *R/V Le Suroît*, the *R/V F.G. Walton Smith* and the *R/V L'Atalante* for  
631 the quality of the data acquired during cruise Carambar 1, 1.5 and 2, and Ifremer-Genavir for cruise  
632 organization and technical support. We also thank TOTAL for their support. We acknowledge IHS for  
633 granting academic Kingdom® software licenses to the University of Bordeaux. Eleanor Georgiadis is  
634 thanked for the English corrections. We thank Ángel Puga-Bernabéu, Erwin Adams and the Associate  
635 Editor, Jim Hendry for insightful reviews.

## REFERENCES

- Augustin, J.-M and Lurton, X.** (2005) Image amplitude calibration and processing for seafloor mapping sonars. *Oceans 2005 - Europe, Conference Paper*, Article number 1511799, Pages 698-701.
- Austin, J., Schlager, W., Palmer, A., Comet, P., Droxler, A., Eberli, G., Fourcade, E., Freeman-Lynde, R., Fulthorpe, C., Harwood, G., Kuhn, G., Lavoie, D., Leckie, M., Melillo, A., Moore, A., Mullins, H., Ravenne, C., Sager, W., Swart, P., Verbeek, J., Watkins, D. and Williams, C.** (1986) Proceedings of the Ocean Drilling Program, Initial Reports Leg. 101.
- Babonneau, N., Savoye, B., Cremer, M. and Klein, B.** (2002) Morphology and architecture of the present canyon and channel system of the Zaire deep-sea fan. *Marine and Petroleum Geology*, 19, 445–467.
- Benson, W.E., Sheridan, R.E., Pastouret, L., Enos, P., Freeman, T., Murdmaa, I.O., Worstell, P., Gradstein, F., Schmidt, R.R., Weaver, F.M. and Stuermer, D.H.** (1978) Initial Reports of the Deep Sea Drilling Project, 44. *U.S. Government Printing Office*.
- Bertello, F., Fantoni, R., Franciosi, R., Gatti, V., Ghielmi, M. and Pugliese, A.** (2010) From thrust-and-fold belt to foreland: hydrocarbon occurrences in Italy. *Geological Society, London, Petroleum Geology Conference series*, 7, 113–126.
- Betzler, C., Lindhorst, S., Eberli, G.P., Lüdmann, T., Möbius, J., Ludwig, J., Schutter, I., Wunsch, M., Reijmer, J.J.G. and Hübscher, C.** (2014) Periplatform drift: The combined result of contour current and off-bank transport along carbonate platforms. *Geology*, 42, 871–874.
- Bryden, H.L., Johns, W.E. and Saunders, P.M.** (2005) Deep western boundary current east of Abaco: Mean structure and transport. *Journal of Marine Research*, 63, 35–57.
- Buchan, K.C.** (2000) The Bahamas. *Marine Pollution Bulletin*, 41, 94–111.
- Busson, J., Joseph, P., Mulder, T., Teles, V., Borgomano, J., Granjeon, D., Betzler, C., Poli, E. and Wunsch, M.** (2019) High-resolution stratigraphic forward modeling of a Quaternary carbonate margin: Controls and dynamic of the progradation. *Sedimentary Geology*, **379**, 77–96.
- Chabaud, L.** (2016) Modèle stratigraphique et processus sédimentaires au Quaternaire sur deux pentes carbonatées des Bahamas (leeward et windward). Université de Bordeaux.

- Chabaud, L., Ducassou, E., Tournadour, E., Mulder, T., Reijmer, J.J.G., Conesa, G., Giraudeau, J., Hanquiez, V., Borgomano, J. and Ross, L.** (2016) Sedimentary processes determining the modern carbonate periplatform drift of Little Bahama Bank. *Marine Geology*, 378, 213–229.
- Coates, A.G., Collins, L.S., Aubry, M.-P. and Berggren, W.A.** (2004) The Geology of the Darien, Panama, and the late Miocene-Pliocene collision of the Panama arc with northwestern South America. *Geological Society of America Bulletin*, 116, 1327–1344.
- Damuth, J.E.** (1980) Use of high-frequency (3.5–12 kHz) echograms in the study of near-bottom sedimentation processes in the deep-sea: A review. *Marine Geology*, 38, 51–75.
- Damuth, J.E. and Hayes, D.E.** (1977) Echo character of the East Brazilian continental margin and its relationship to sedimentary processes. *Marine Geology*, 24, 73–95.
- Duncan, R.A. and Hargraves, R.B.** (1984) Plate tectonic evolution of the Caribbean region in the mantle reference frame. *Geological Society of America Memoirs*, 162, 81–94.
- Engebretson, D.C., Cox, A. and Gordon, R.G.** (1985) Relative Motions Between Oceanic and Continental Plates in the Pacific Basin. *Geological Society of America Special Papers*, 206, 1–60.
- Enos, P.** (1974) Surface sediment facies of the Florida-Bahamas Plateau. Geological Society of America Map. *Geological Society of America*.
- Fauquembergue, K.** (2018) Transferts sédimentaires sur une marge carbonatémoyenne de la plate-forme à la plaine abyssale : marge nord de Little Bahama Bank, Bahamas. Université de Bordeaux.
- Fauquembergue, K., Ducassou, E., Mulder, T., Hanquiez, V., Perello, M.-C., Poli, E. and Borgomano, J.** (2018) Genesis and growth of a carbonate Holocene wedge on the northern Little Bahama Bank. *Marine and Petroleum Geology*, 96, 602–614.
- Guiastrennec-Faugas, L., Gillet, H., Jacinto, R.S., Dennielou, B., Hanquiez, V., Schmidt, S., Simplet, L. and Rousset, A.** (2020) Upstream migrating knickpoints and related sedimentary processes in a submarine canyon from a rare 20-year morphobathymetric time-lapse (Capbreton submarine canyon, Bay of Biscay, France). *Marine Geology*, 106143.
- Hanquiez, V., Mulder, T., Lecroart, P., Gonthier, E., Marchès, E. and Voisset, M.** (2007) High resolution seafloor images in the Gulf of Cadiz, Iberian margin. *Marine Geology*, 246, 42–59.

- Hanquiez, V., Mulder, T., Toucanne, S., Lecroart, P., Bonnel, C., Marchès, E. and Gonthier, E.** (2010) The sandy channel-lobe depositional systems in the Gulf of Cadiz: Gravity processes forced by contour current processes. *Sedimentary Geology*, 229, 110–123.
- Hardy, J.W. and Henderson, K.G.** (2003) Cold Front Variability in the Southern United States and the Influence of Atmospheric Teleconnection Patterns. *Physical Geography*, 24, 120–137.
- Hine, A.C. and Neumann, A.C.** (1977) Shallow Carbonate-Bank-Margin Growth and Structure, Little Bahama Bank, Bahamas. *AAPG Bulletin*, 61, 376–406.
- Hine, A.C., Wilber, R.J., Bane, J.M., Neumann, A.C. and Lorenson, K.R.** (1981) Offbank transport of carbonate sands along open, leeward bank margins: Northern Bahamas. *Marine Geology*, 42, 327–348.
- Hollister, C.D., Flood, R.D., Johnson, D.A., Lonsdale, P. and Southard, J.B.** (1974) Abyssal Furrows and Hyperbolic Echo Traces on the Bahama Outer Ridge. *Geology*, 2, 395–400.
- Hollister, C.D. and Heezen, B.C.** (1972) Geologic effects of ocean bottom currents: Western North Atlantic. *Woods Hole Oceanographic Institution*.
- James, K.H.** (2009) Evolution of Middle America and the in situ Caribbean Plate model. *Geological Society, London, Special Publications*, 328, 127–138.
- Johns, W.E., Kanzow, T. and Zantopp, R.** (2005) Estimating ocean transports with dynamic height moorings: An application in the Atlantic Deep Western Boundary Current at 26°N. *Deep Sea Research Part I: Oceanographic Research Papers*, 52, 1542–1567.
- Komar, P.D.** (1971) Hydraulic Jumps in Turbidity Currents. *GSA Bulletin*, 82, 1477–1488.
- Lee, T.N., Johns, W.E., Zantopp, R.J. and Fillenbaum, E.R.** (1996) Moored Observations of Western Boundary Current Variability and Thermohaline Circulation at 26.5° in the Subtropical North Atlantic. *J. Phys. Oceanogr.*, 26, 962–983.
- Meinen, C.S., Garzoli, S.L., Johns, W.E. and Baringer, M.O.** (2004) Transport variability of the Deep Western Boundary Current and the Antilles Current off Abaco Island, Bahamas. *Deep Sea Research Part I: Oceanographic Research Papers*, 51, 1397–1415.



- Meschede, M. and Frisch, W.** (1998) A plate-tectonic model for the Mesozoic and Early Cenozoic history of the Caribbean plate. *Tectonophysics*, 296, 269–291.
- Mulder, T., Ducassou, E., Eberli, G.P., Hanquiez, V., Gonthier, E., Kindler, P., Principaud, M., Fournier, F., Leonide, P., Billeaud, I., Marsset, B., Reijmer, J.J.G., Bondu, C., Joussiaume, R. and Pakiades, M.** (2012a) New insights into the morphology and sedimentary processes along the western slope of Great Bahama Bank. *Geology*, 40, 603–606.
- Mulder, T., Ducassou, E., Gillet, H., Hanquiez, V., Tournadour, E., Combes, J., Eberli, G.P., Kindler, P., Gonthier, E., Conesa, G., Robin, C., Sianipar, R., Reijmer, J.J.G. and François, A.** (2012b) Canyon morphology on a modern carbonate slope of the Bahamas: Evidence of regional tectonic tilting. *Geology*, 771-774.
- Mulder, T., Ducassou, E., Gillet, H., Hanquiez, V., Principaud, M., Chabaud, L., Eberli, G.P., Kindler, P., Billeaud, I., Gonthier, E., Fournier, F., Léonide, P. and Borgomano, J.** (2014) First discover of channel-levee complexes in a modern deep-water carbonate slope environment. *Journal of Sedimentary Reserarch*, V.84, 1139 to 1146.
- Mulder, T., Joumes, M., Hanquiez, V., Gillet, H., Reijmer, J.J.G., Tournadour, E., Chabaud, L., Principaud, M., Schnyder, J.S.D., Borgomano, J., Fauquembergue, K., Ducassou, E. and Busson, J.** (2017) Carbonate slope morphology revealing sediment transfer from bank-to-slope (Little Bahama Bank, Bahamas). *Marine and Petroleum Geology*, 83, 26–34.
- Mulder, T., Gillet, H., Hanquiez, V., Ducassou, E., Fauquembergue, K., Principaud, M., Conesa, G., Goff, J.L., Ragusa, J., Bashah, S., Bujan, S., Reijmer, J.J.G., Cavailhes, T., Droxler, A.W., Blank, D.G., Guiastrennec, L., Fabregas, N., Recouvreur, A. and Seibert, C.** (2018) Carbonate slope morphology revealing a giant submarine canyon (Little Bahama Bank, Bahamas). *Geology*, 46, 31–34.
- Mullins, H.T., Heath, K.C., Van Buren, H.M. and Newton, C.R.** (1984) Anatomy of a modern open-ocean carbonate slope: northern Little Bahama Bank. *Sedimentology*, 31, 141–168.
- Mullins, H.T., Keller, G.H., Kofoed, J.W., Lambert, D.N., Stubblefield, W.L. and Warme, J.E.** (1982) Geology of Great Abaco Submarine Canyon (Blake Plateau): Observations from the research submersible “Alvin”. *Marine Geology*, 48, 239–257.

- Mullins, H.T. and Neumann, A.C.** (1979) Deep Carbonate Bank Margin Structure and Sedimentation in the Northern Bahamas. *Soc. Econ. Paleontologists Mineralogists Spec. Pub*, 165–192.
- Mullins, H.T., Neumann, A.C., Wilber, R.J., Hine, A.C. and Chinburg (S), S.J.** (1980) Carbonate Sediment Drifts in Northern Straits of Florida. *AAPG Bulletin*, 64, 1701–1717.
- Neumann, G. and Pierson, W.J.J.** (1966) Principles of physical oceanography. *Englewood Cliffs, NJ (USA) Prentice Hall*.
- Paull, C., Caress, D., Lundsten, E., Gwiazda, R., Anderson, K., McGann, M., Conrad, J., Edwards, B. and Sumner, E.** (2013) Anatomy of the La Jolla submarine canyon system; offshore Southern California. *Marine Geology*, 335, 16–34.
- Pindell, J.L.** (1994) Evolution of the Gulf of Mexico and the Caribbean. *Caribbean geology: an introduction*, 13–39.
- Principaud, M., Mulder, T., Hanquiez, V., Ducassou, E., Eberli, G.P., Chabaud, L. and Borgomano, J.** (2018) Recent morphology and sedimentary processes along the western slope of Great Bahama Bank (Bahamas). *Sedimentology*, 65, 2088–2116.
- Puga-Bernabéu, Á., Webster, J.M., Beaman, R.J. and Guilbaud, V.** (2011) Morphology and controls on the evolution of a mixed carbonate–siliciclastic submarine canyon system, Great Barrier Reef margin, north-eastern Australia. *Marine Geology*, 289, 100–116.
- Rankey, E.C. and Doolittle, D.F.** (2012) Geomorphology of carbonate platform-marginal uppermost slopes: Insights from a Holocene analogue, Little Bahama Bank, Bahamas. *Sedimentology*, 59, 2146–2171.
- Reeder, S.L. and Rankey, E.C.** (2009) Controls on morphology and sedimentology of carbonate tidal deltas, Abacos, Bahamas. *Marine Geology*, 267, 141–155.
- Reijmer, J.J.G., Palmieri, P. and Groen, R.** (2012) Compositional variations in calciturbidites and calcidebrites in response to sea-level fluctuations (Exuma Sound, Bahamas). *Facies*, 58, 493–507.
- Richardson, P.L.** (1977) On the crossover between the Gulf Stream and the Western Boundary Undercurrent. *Deep Sea Research*, 24, 139–159.

- Ross, M.I. and Scotese, C.R.** (1988) A hierarchical tectonic model of the Gulf of Mexico and Caribbean region. *Tectonophysics*, 155, 139–168.
- Schlager, W.** (2005) Carbonate Sedimentology and Sequence Stratigraphy. *SEPM Soc for Sed Geology*, 210 pp.
- Shepard and Dill** (1966) Submarine canons and Other Sea Valleys. *Rand Mc.ally & Company*.
- Sheridan, R., Mullins, H., Austin Jr, J., Ball, M., Ladd, J. and Grow, J.** (1988a) Geology and geophysics of the Bahamas. *The Geology of North America*, 1, 2.
- Sheridan, R.E., Mullins, H.T., Austin Jr, J.A., Ball, M.M., Ladd, J.W. and Grow, J.A.** (1988b) Geology and geophysics of the Bahamas. *The Geology of North America*, 1, 2.
- Sheridan, R.E. and Osburn, W.L.** (1975) Marine Geological and Geophysical Studies of the Florida - Blake Plateau - Bahamas Area. 9–32.
- Tournadour, E.** (2015) Architecture et dynamique sédimentaire d'une pente carbonatée moderne : exemple de la pente nord de Little Bahama Bank (LBB), Bahamas. Université de Bordeaux.
- Tournadour, E., Mulder, T., Borgomano, J., Hanquiez, V., Ducassou, E. and Gillet, H.** (2015) Origin and architecture of a Mass Transport Complex on the northwest slope of Little Bahama Bank (Bahamas): Relations between off-bank transport, bottom current sedimentation and submarine landslides. *Sedimentary Geology*, 317, 9–26.
- Tournadour, E., Mulder, T., Borgomano, J., Gillet, H., Chabaud, L., Ducassou, E., Hanquiez, V. and Etienne, S.** (2017) Submarine canyon morphologies and evolution in modern carbonate settings: The northern slope of Little Bahama Bank, Bahamas. *Marine Geology*, 391, 76–97.
- Tubau, X., Paull, C.K., Lastras, G., Caress, D.W., Canals, M., Lundsten, E., Anderson, K., Gwiazda, R. and Amblas, D.** (2015) Submarine canyons of Santa Monica Bay, Southern California: Variability in morphology and sedimentary processes. *Marine Geology*, 365, 61–79.
- Wilson, P.A. and Roberts, H.H.** (1992) Carbonate-periplatform sedimentation by density flows: A mechanism for rapid off-bank and vertical transport of shallow-water fines. *Geology*, 20, 713.
- Wilson, P.A. and Roberts, H.H.** (1995) Density cascading: Off-shelf sediment transport, evidence and implications, Bahama Banks. *Journal of Sedimentary Research*, 45–56.

## FIGURE CAPTIONS

Fig. 1. Geographical context of the study including Carambar 1 Leg 2, Carambar 1.5 and Carambar 2 Leg 1 survey location. GAC = Great Abaco Canyon; LAC = Little Abaco Canyon; GAFZ = Great Abaco Fracture Zone (thin grey line); DWBC = Deep Western Boundary Current; AABW = Antarctic Bottom Water.

Fig. 2. **(A)** Overview of Little Bahama Bank (LBB) slope morphology evidenced by bathymetric data. Black squares show the locations of subsequent figures and tables. Location of the different slope domain limits is also shown. **(B)** Three-dimensional east–west view of the study area. White lines: location of different slope domain limits. Black and blue dashed lines = location of profiles in **(C)**. Vertical exaggeration  $\times 3$ . **(C)** Little Bahama Bank slope profiles with respective slope domains. GAC = Great Abaco Canyon; LAC = Little Abaco Canyon; MWD = mass wasting deposits; sw = sediment waves; s = slides; MTC = mass transport complex.

Fig. 3. **(A)** Close-up of the bathymetry of the slope canyons with an up dip linear part (see location on Fig. 2). Canyon flanks represented in black lines. **(B)** High resolution bathymetry of the mounds and pockmarks with associated profiles.

Fig. 4. Distinctive morphological features of the Little Bahama Bank (LBB) lower slope (see location on Fig. 2). **(A)** Close up of cross-cutting furrows F1 and F2 affecting the lower slope. **(B)** Close-up of the sediment waves (SW; dotted black line; graphic representing depth profile) over the lobe (dotted red line) at an eastern slope canyon mouth. **(C)** Close-up of the slides (S) affecting the Great Abaco Canyon flanks. **(D)** Close-up of the Little Abaco Canyon mouth showing the location of the sediment lobe (LAC Lobe).

Fig. 5. **(A)** Close-up of the Great Abaco Canyon and the Little Abaco Canyon and depth profile locations (see location on Fig. 2). **(B)** North–south profiles of the Great Abaco Canyon and the Little Abaco Canyon displaying U shaped canyons. **(C)** Little Abaco Canyon longitudinal depth profile. **(D)** Great Abaco Canyon longitudinal depth profile. PP = plunge pool; kn = knickpoint.

Fig. 6. High resolution bathymetry of the distal part of the canyons showing the plunge pools (white dashed lines) of the Great Abaco Canyon **(A)** and Little Abaco Canyon **(B)**.

Fig. 7. Backscatter map of the northern Little Bahama Bank (LBB) slope. White boxes represent the location of the acoustic facies and echofacies summarized in Table 1.

Fig. 8. Acoustic facies distribution on the northern Little Bahama Bank (LBB) slope.

Fig. 9. Echofacies distribution on the northern Little Bahama Bank (LBB) slope.

Fig. 10. Synthetic map of the northern Little Bahama Bank (LBB) slope sedimentary processes (**C**) obtained by the integration of acoustic facies (**A**) and echofacies (**B**) distributions.

Fig. 11. Synthetic map of the Little Bahama Bank (LBB) slope sedimentary processes. Cold colours (first column) represent processes and geometries mainly generated by deposition. Warm colours (second column) represent processes and geometries mainly influenced by erosion. The third column represents platform facies [from Enos (1974) and modified by Tournadour (2015)].

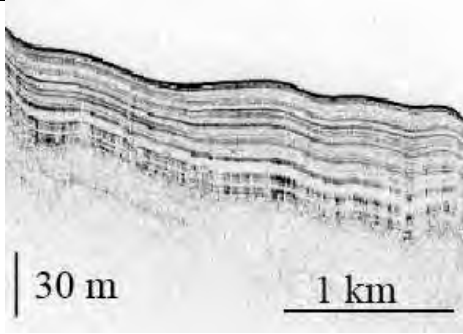
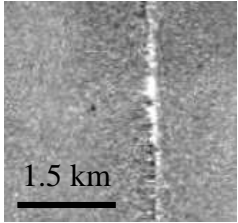

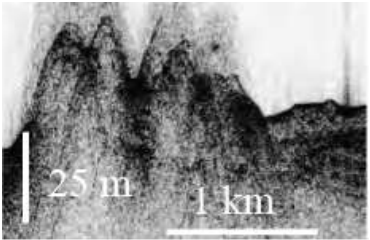
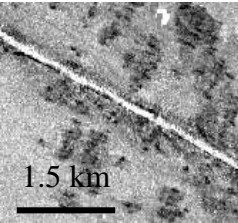

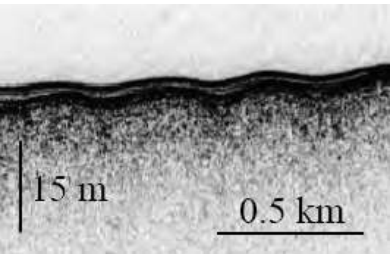
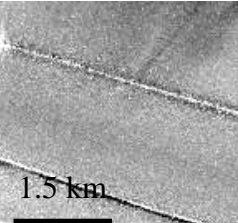

Fig. 12. Three-dimensional views (vertical exaggeration x3) of (**A**) the Little Bahama Bank (LBB) slope environments and (**B**) of the conceptual model of the sedimentary processes on the northern LBB slope; platform facies from Enos (1974) and modified by Tournadour (2015). GAC = Great Abaco Canyon; LAC = Little Abaco Canyon; DWBC = Deep Western Boundary Current.

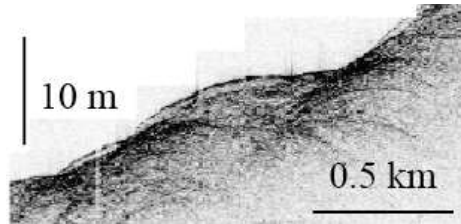
Fig. 13. High resolution bathymetry of (**A**) the Great Abaco Canyon head and (**B**) of the eastern canyons. GAC = Great Abaco Canyon.

Table 1. Sedimentary facies interpretations using both acoustic facies, echofacies and bathymetry. Location of the acoustic facies on Fig. 7. The Very High Resolution (VHR) facies are located at the same place as the reflectivity data.

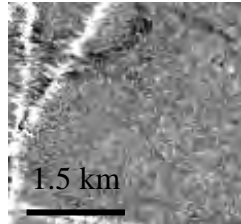
Table 2. Classification and description of acoustic facies.

Table 3. Classification and description of echofacies.

VHR seismic	Backscatter	Facies	Legend	Facies number
 <p data-bbox="421 568 519 595">Bedded</p>	 <p data-bbox="792 512 1097 544">Medium Homogeneous</p>	Hemipelagic sedimentation		1
 <p data-bbox="398 871 542 898">Hyperbolic</p>	 <p data-bbox="792 847 1097 916">Medium Heterogeneous patchy</p>	Carbonate mounds		2
 <p data-bbox="434 1197 510 1224">Blind</p>	 <p data-bbox="792 1203 1097 1235">Medium Homogeneous</p>	Periplatform ooze deposits		3



Combined I (blind + hyperbolic)

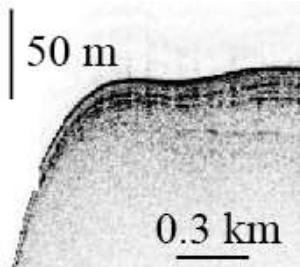


Medium Homogeneous

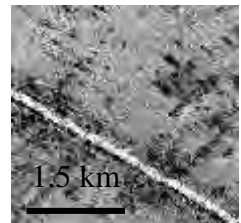
Turbidites



4



Bedded/blind

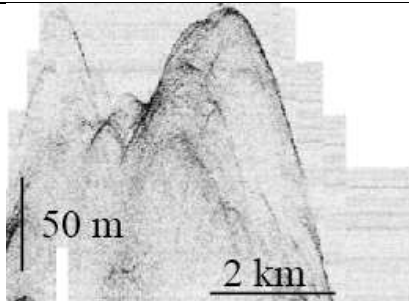


Medium Punctuated  
Heterogeneous

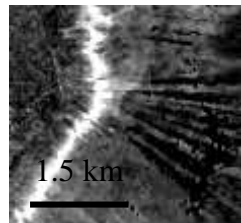
Base of slope  
deposits



5



Hyperbolic

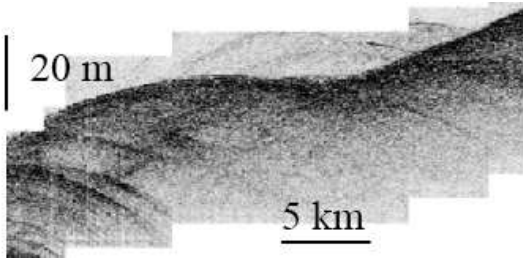


Very High Heterogeneous

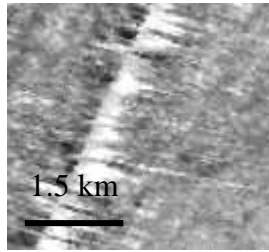
Mass wasting  
deposits



6



Combined I (hyperbolic + blind)

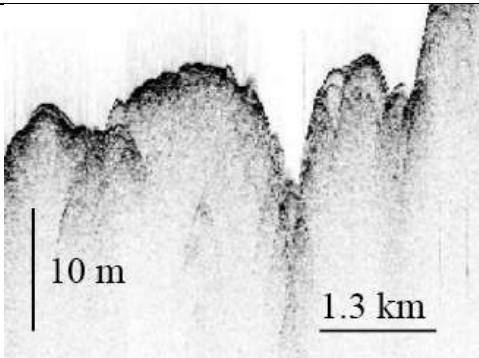


Medium Homogeneous

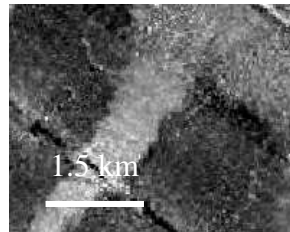
Abyssal plain



7



Hyperbolic

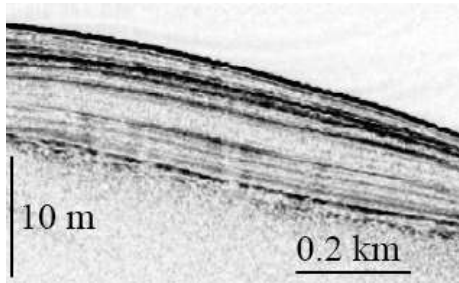


Medium Homogeneous

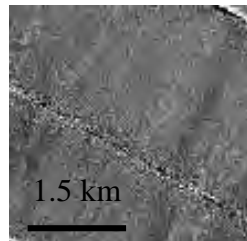
Canyons



8



Bedded



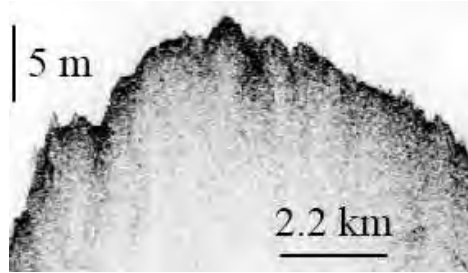
High Homogeneous

Nodular ooze

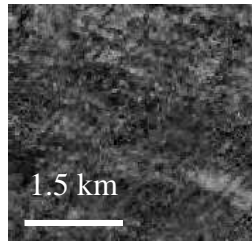


9





Blind

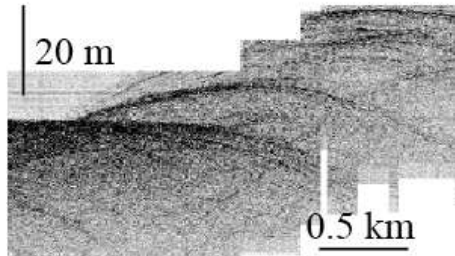


High Heterogeneous

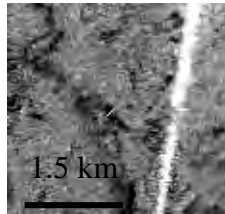
Hardground



10



Hyperbolic

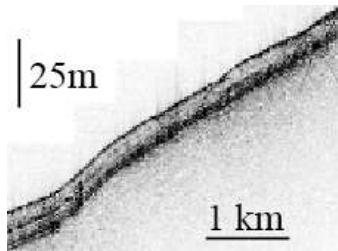


Medium Heterogeneous  
Punctuated

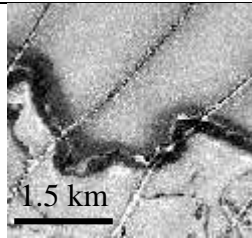
Slides



11



Bedded

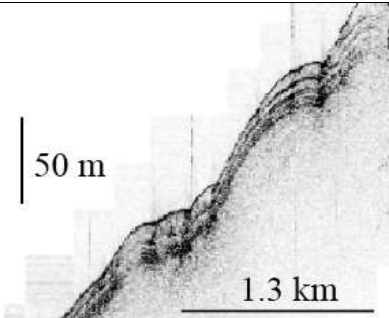


Very High Homogeneous  
Followed by Medium  
Homogeneous

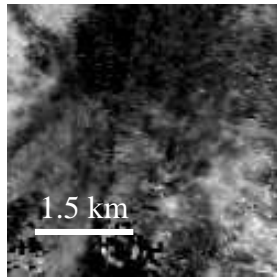
MTC Hardground



12



Combined II (hyperbolic+bedded)

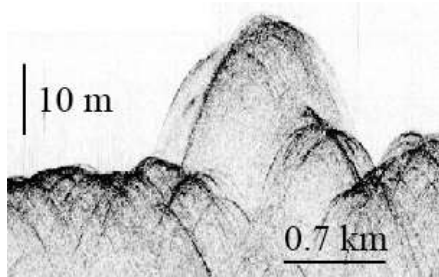


Very High Heterogeneous

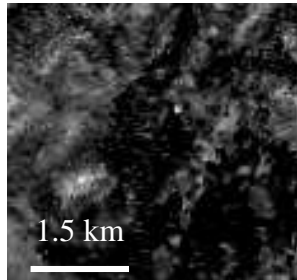
GAC,LAC,  
tributaries



13



Hyperbolic


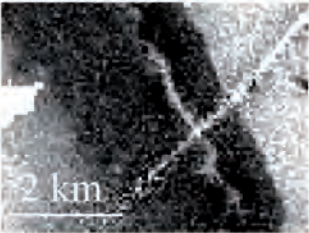

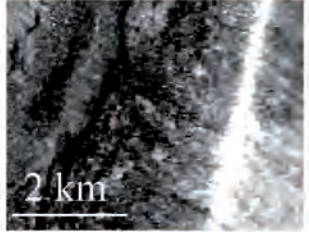
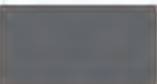
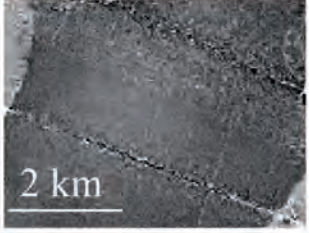

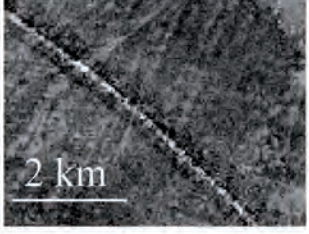



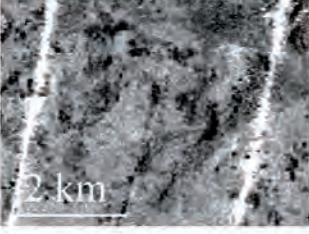

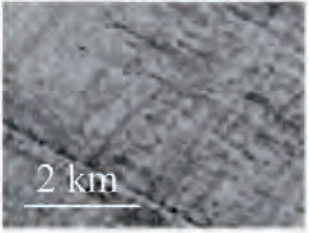

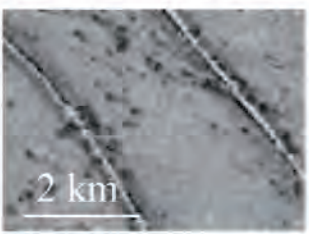


Very High Heterogeneous

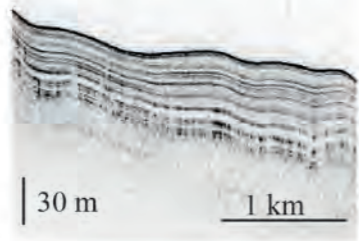
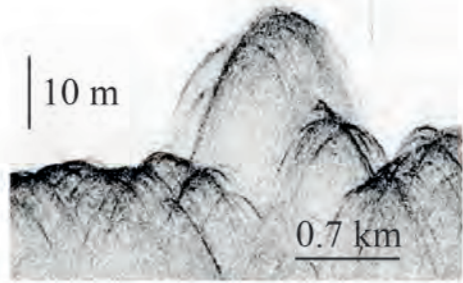
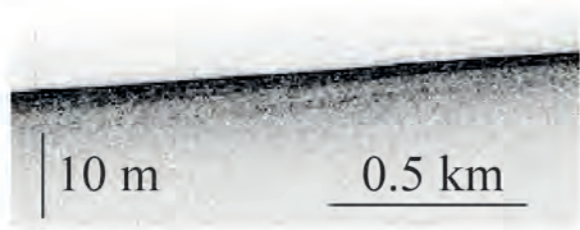
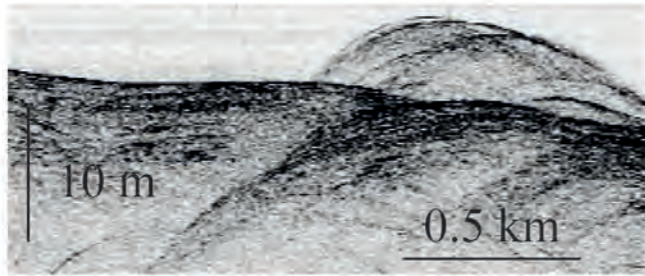
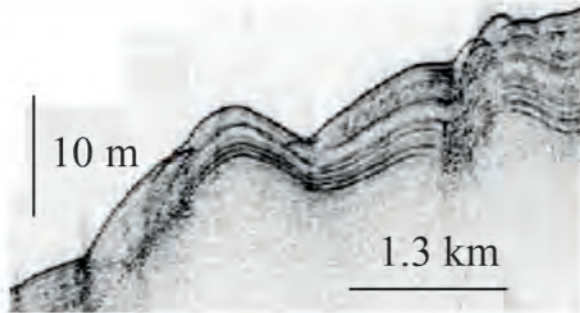
BBE



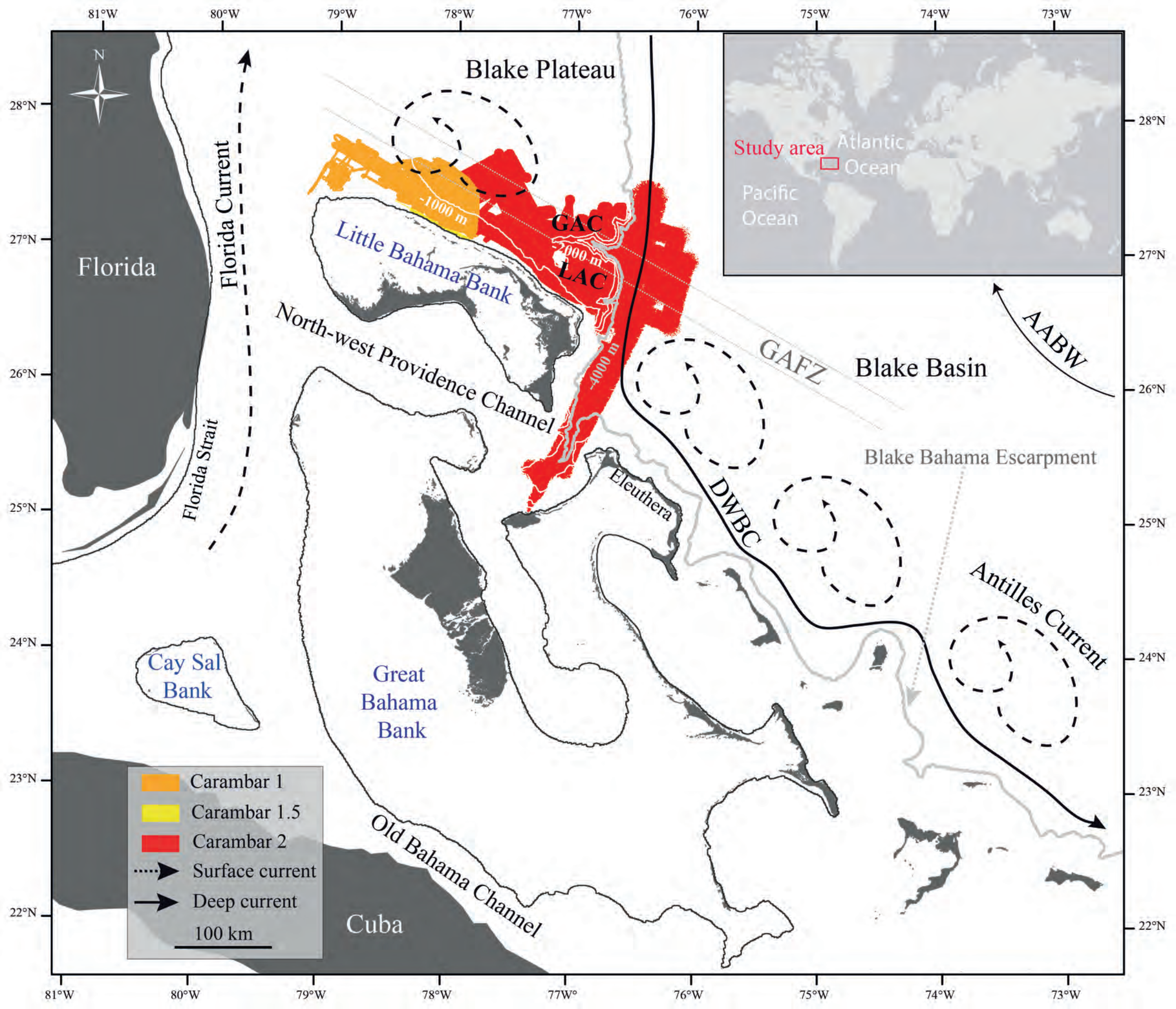
14

Legend	Backscatter	Facies	Description
		Very high homogenous	Very high homogenous reflectivity
		Very-high heterogeneous	Very-high reflectivity with patches of high reflectivity
		High homogeneous	High homogeneous reflectivity
		High heterogeneous	High reflectivity with medium reflectivity lineations
		Medium homogeneous	Medium homogeneous reflectivity
		Medium patchy heterogeneous	Medium reflectivity with patches of high reflectivity
		Medium undulated heterogeneous	Medium reflectivity with high reflectivity undulated structures
		Medium punctuated heterogeneous	Medium reflectivity with small circular patches of high reflectivity

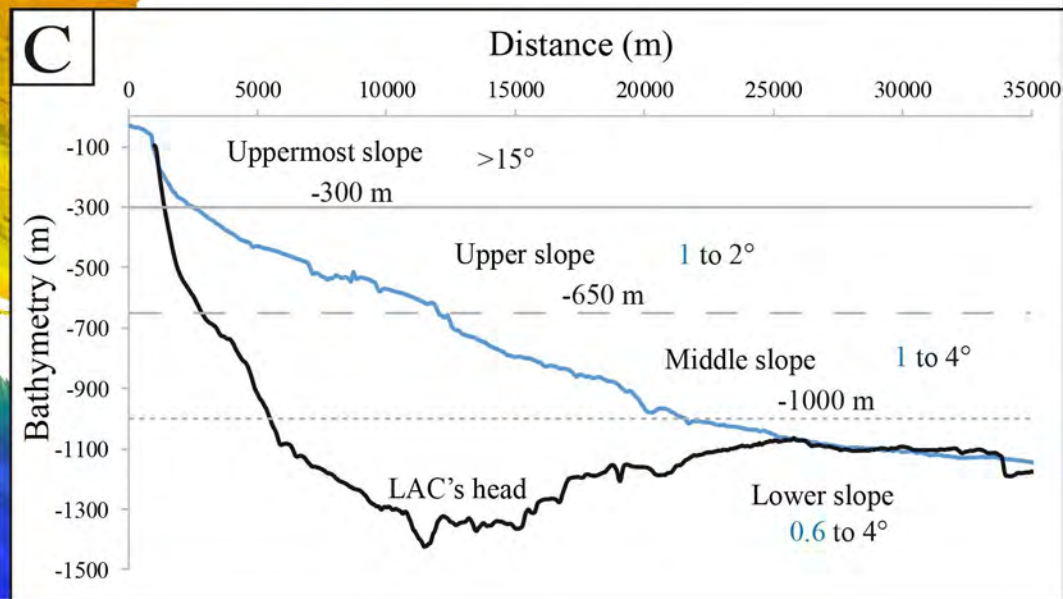
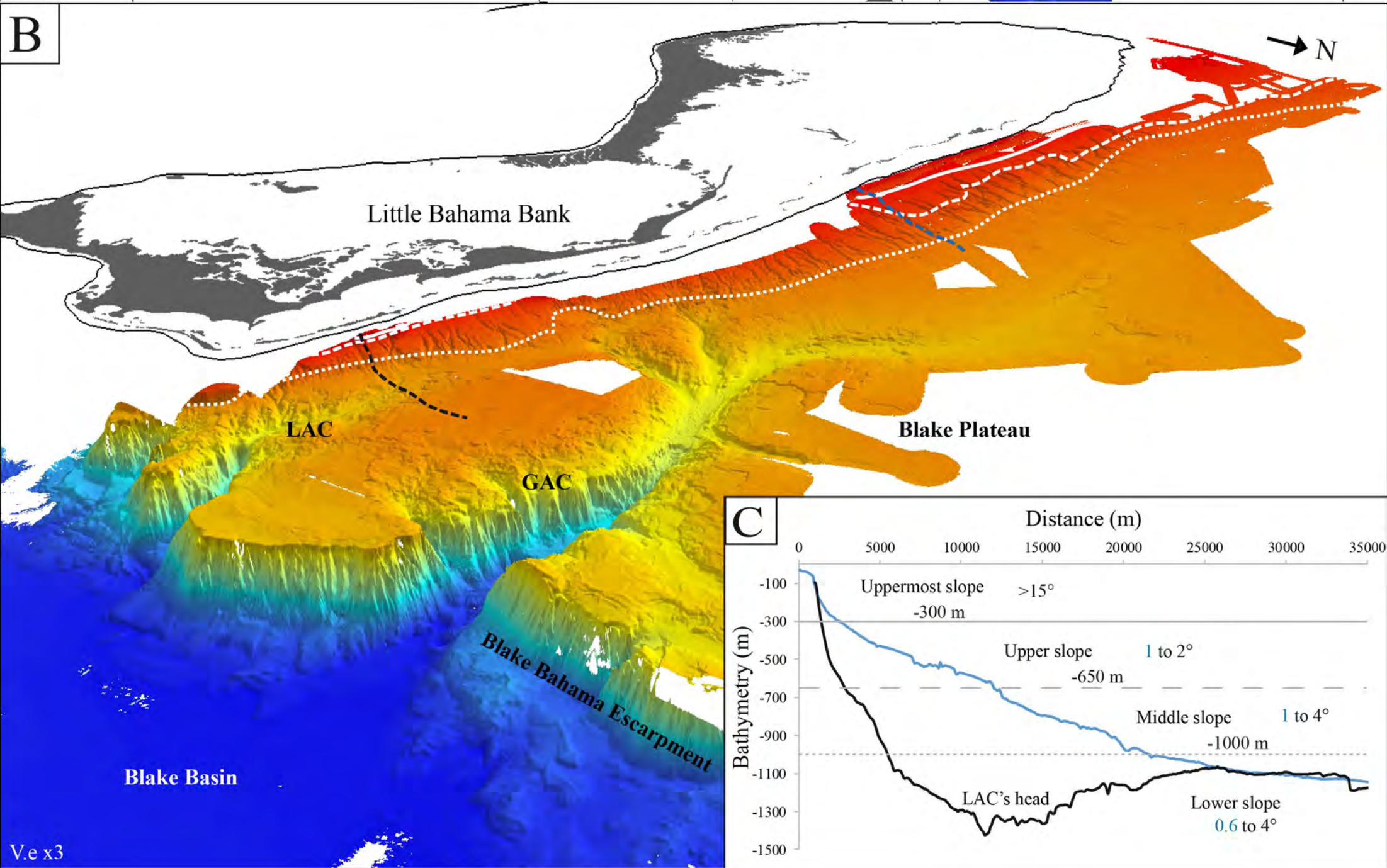
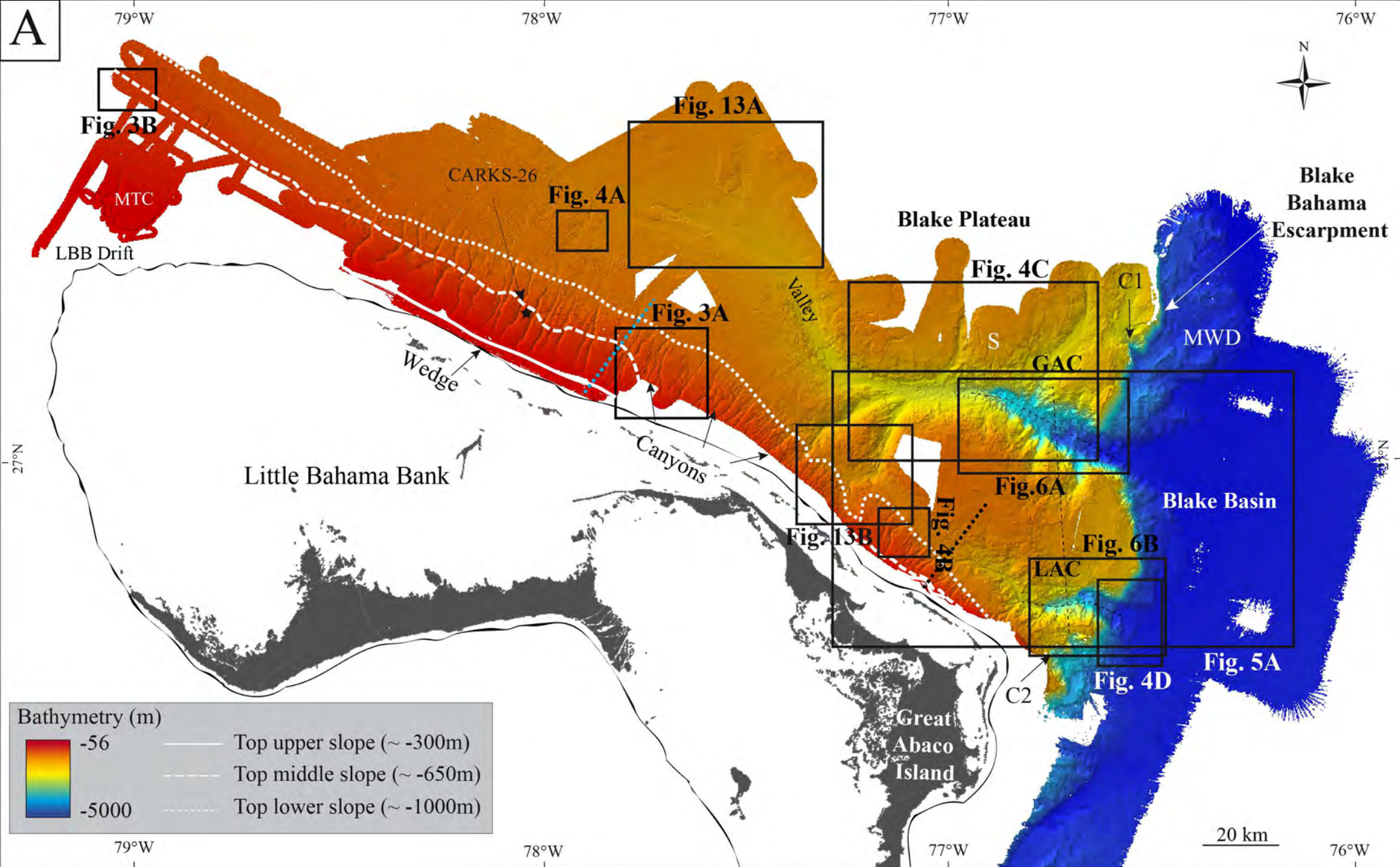


Legend	Very High Resolution Seismic (VHR)	Echofacies	Description
1		Bedded	Continuous parallel low to high amplitude reflectors
2		Hyperbolic	Chaotic hyperbolic-shaped high amplitude reflectors
3		Blind	Surficial reflector of very-high amplitude with diffuse facies (underlying reflectors cannot be identified)
4		Combined I (Hyperbolic + blind)	High amplitude hyperbolic-shaped reflectors which are less defined and more diffuse with depth
5		Combined II (Hyperbolic + bedded)	Parallel continuous low to high amplitude reflectors extending from hyperbolic-shaped reflectors

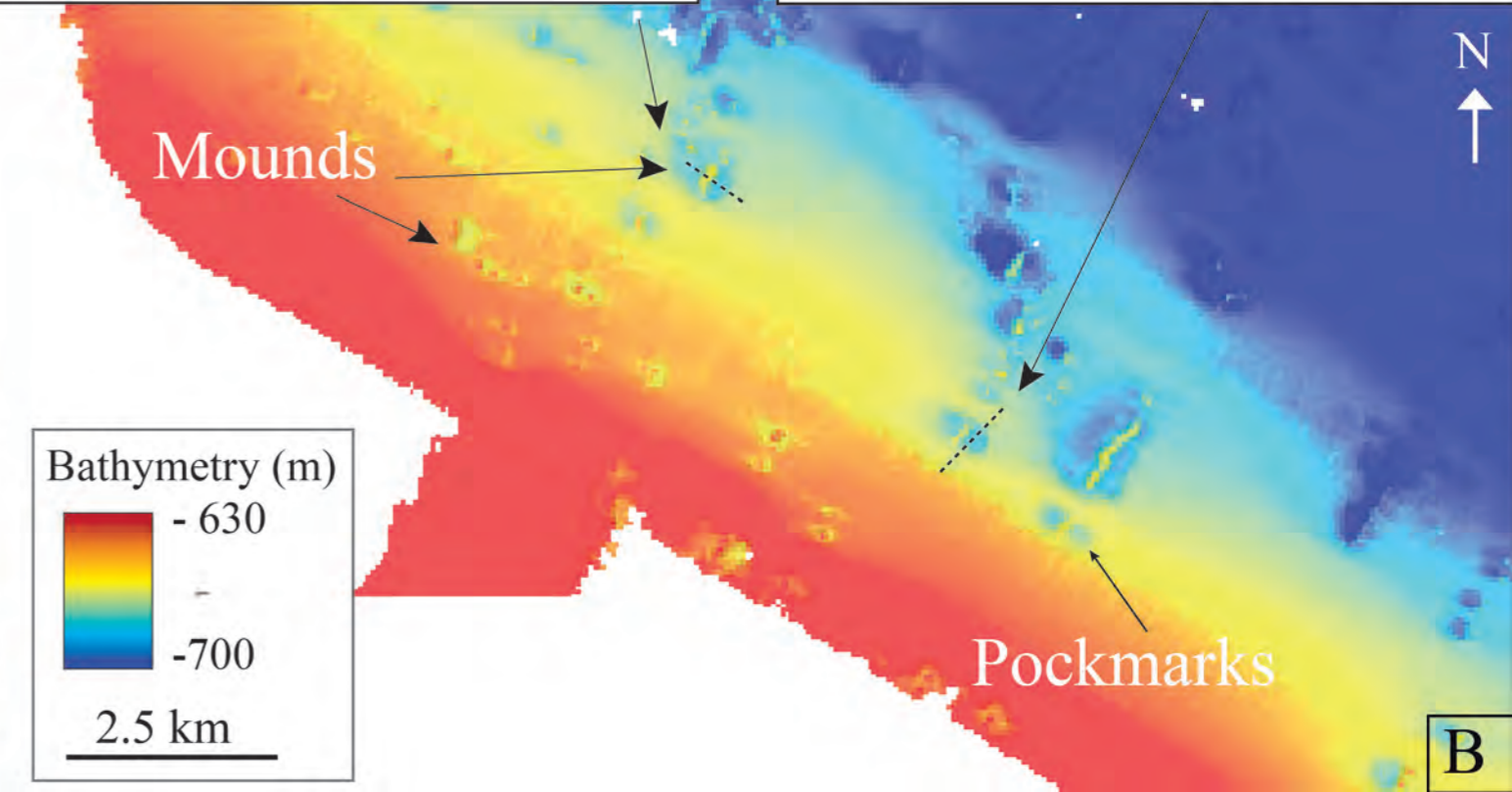
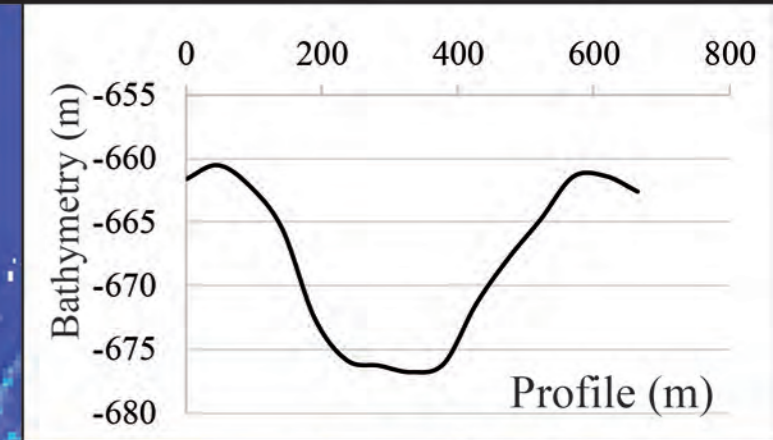
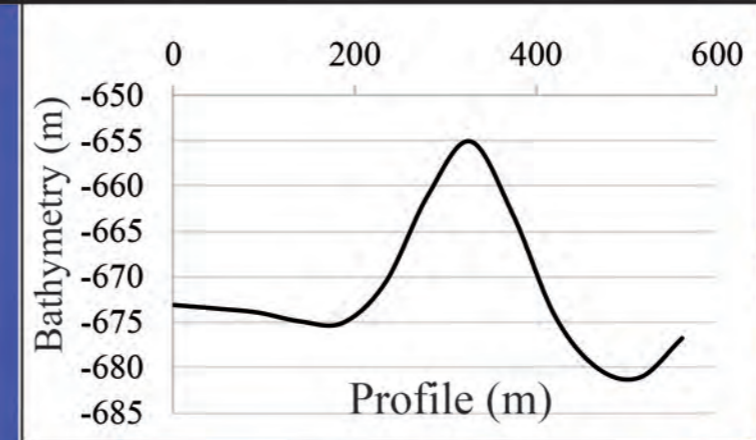
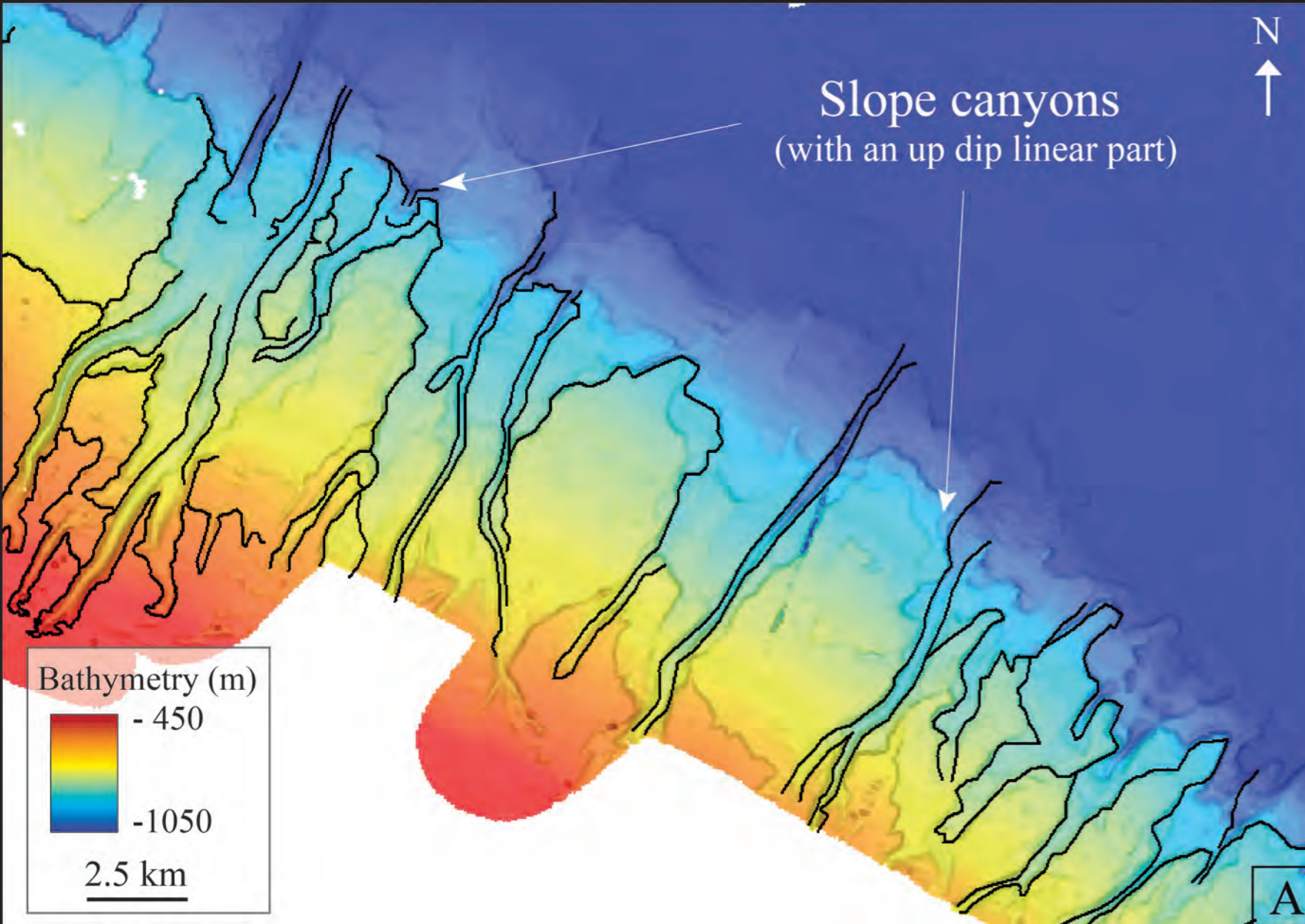




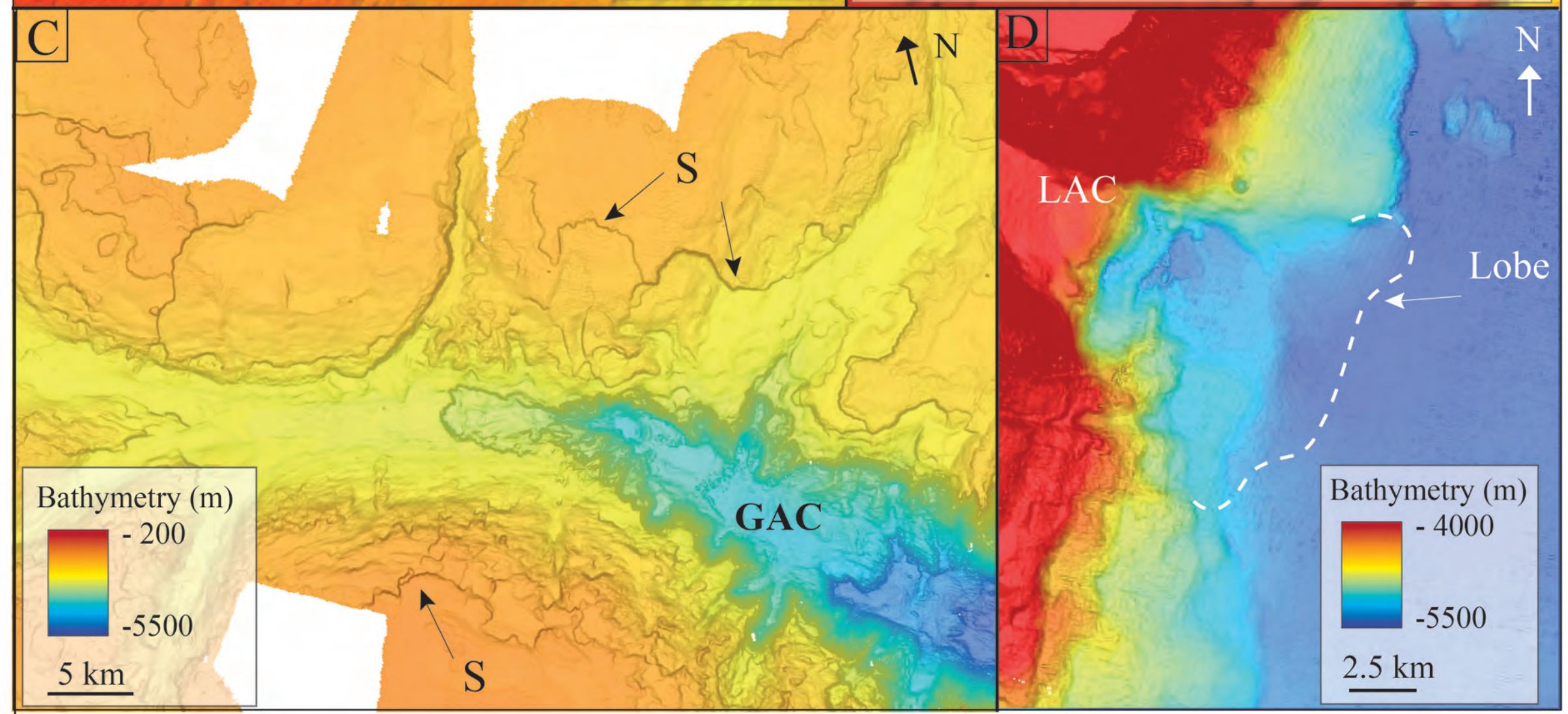
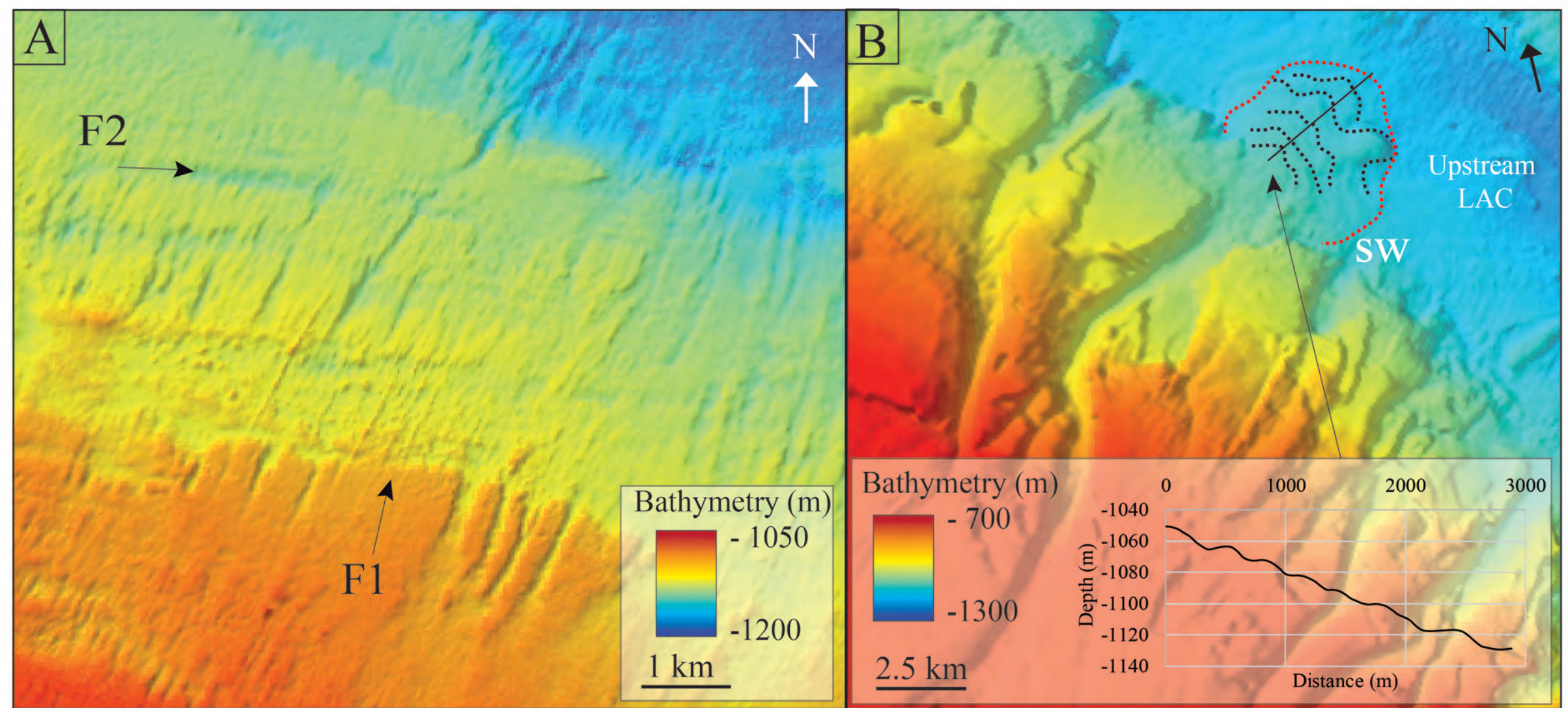




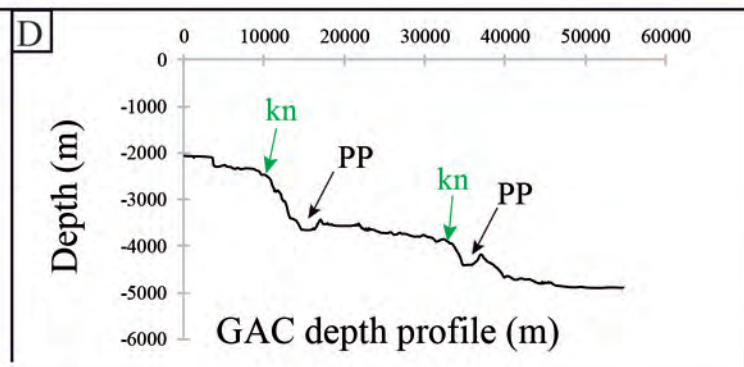
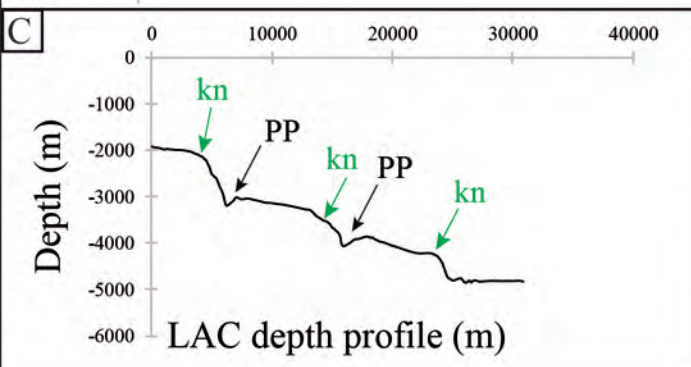
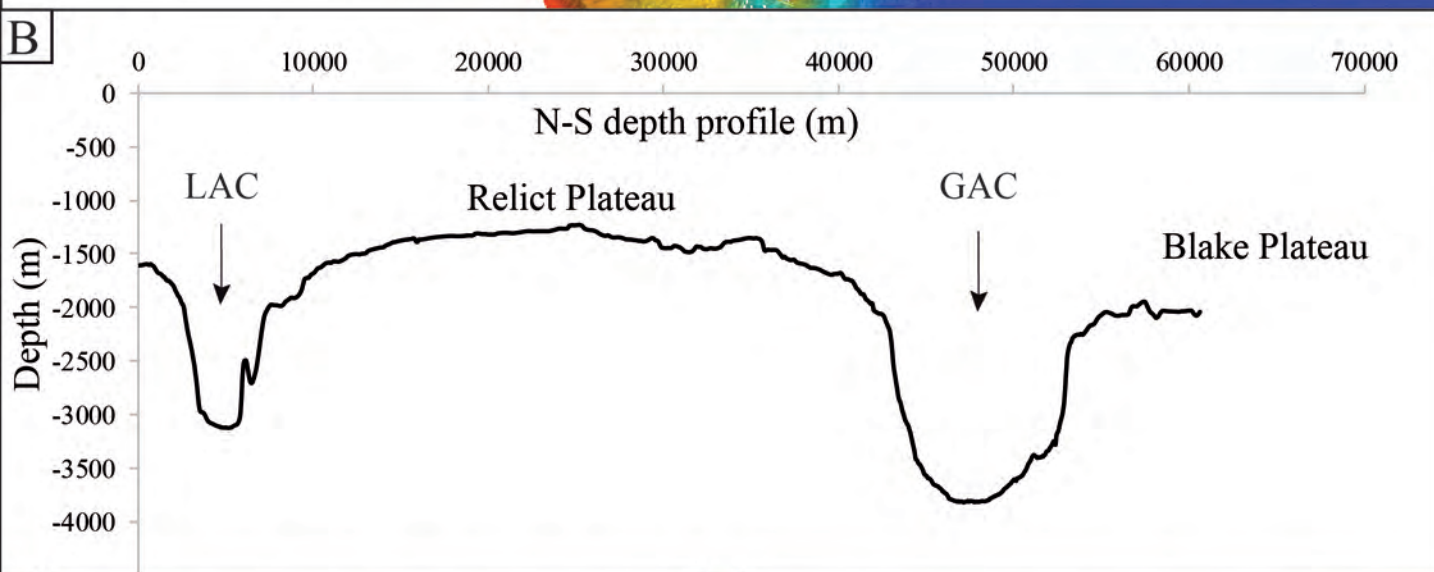
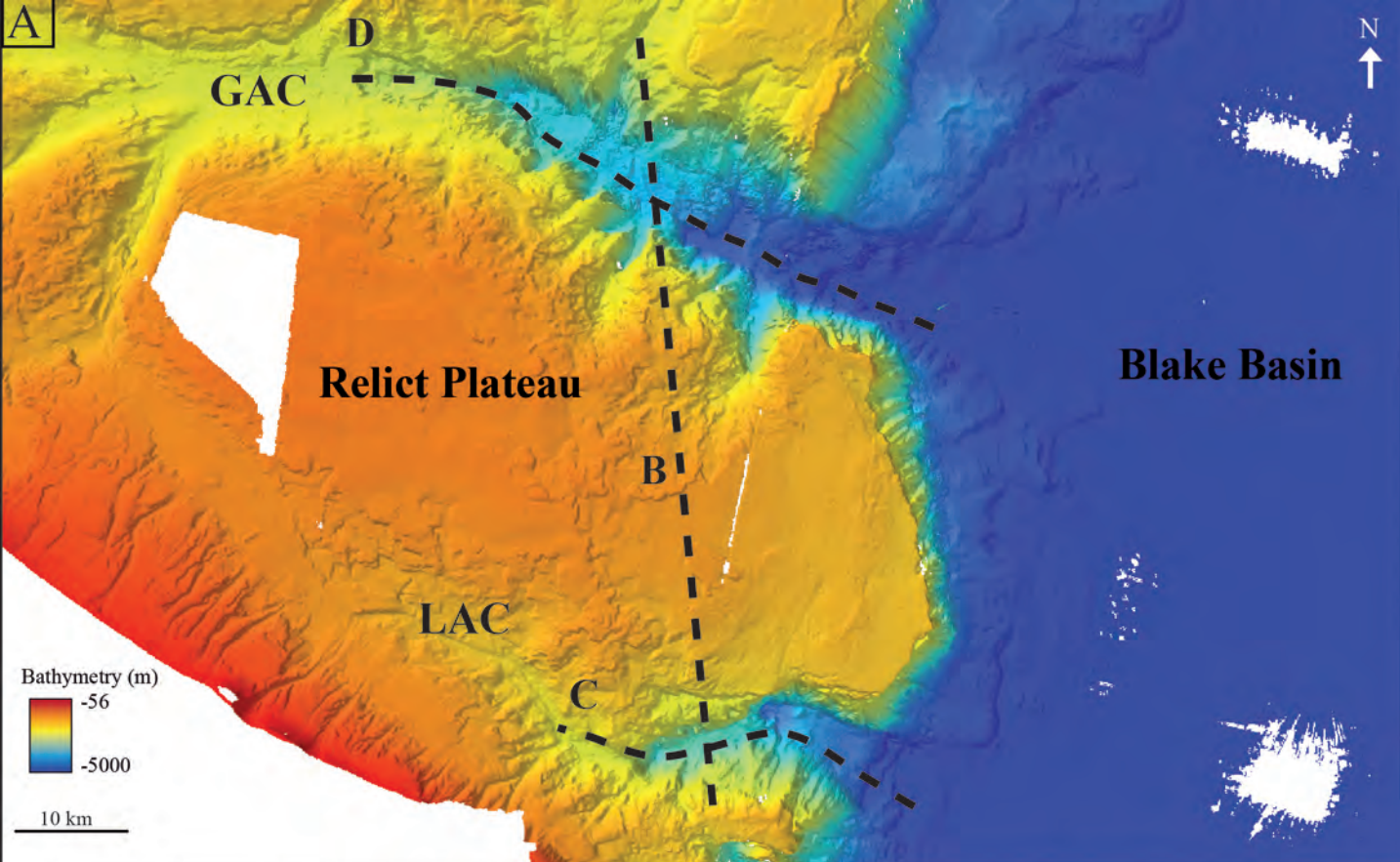




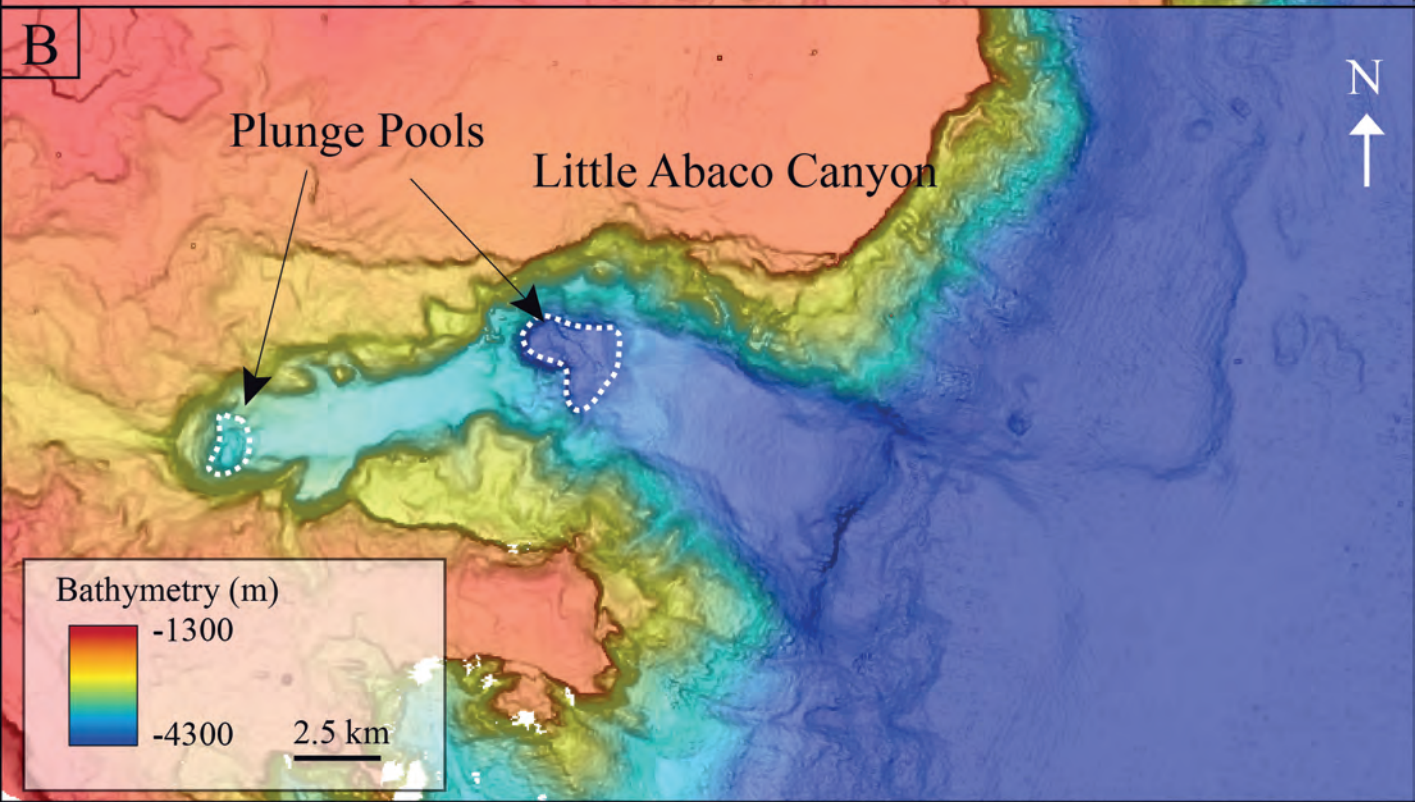
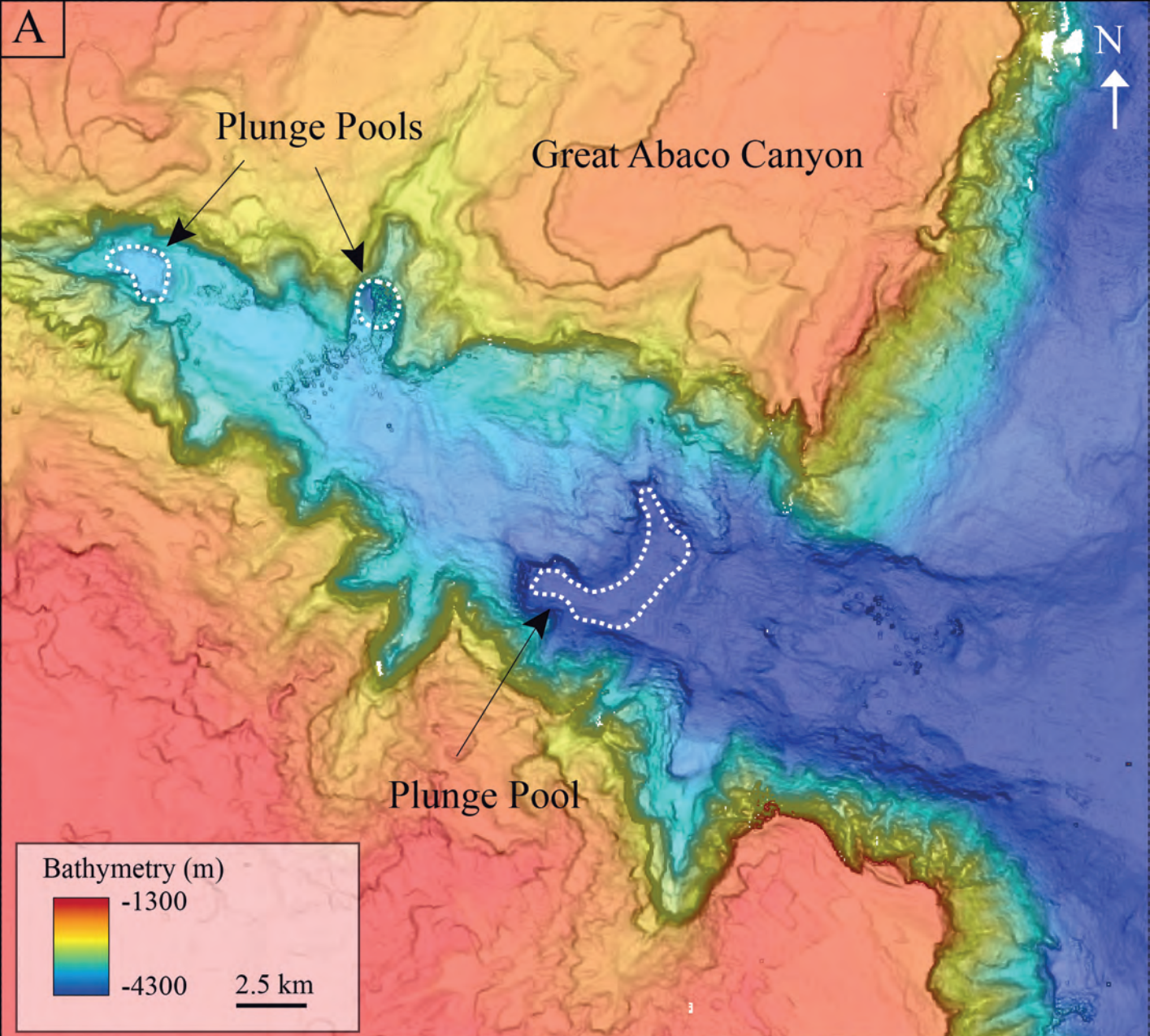








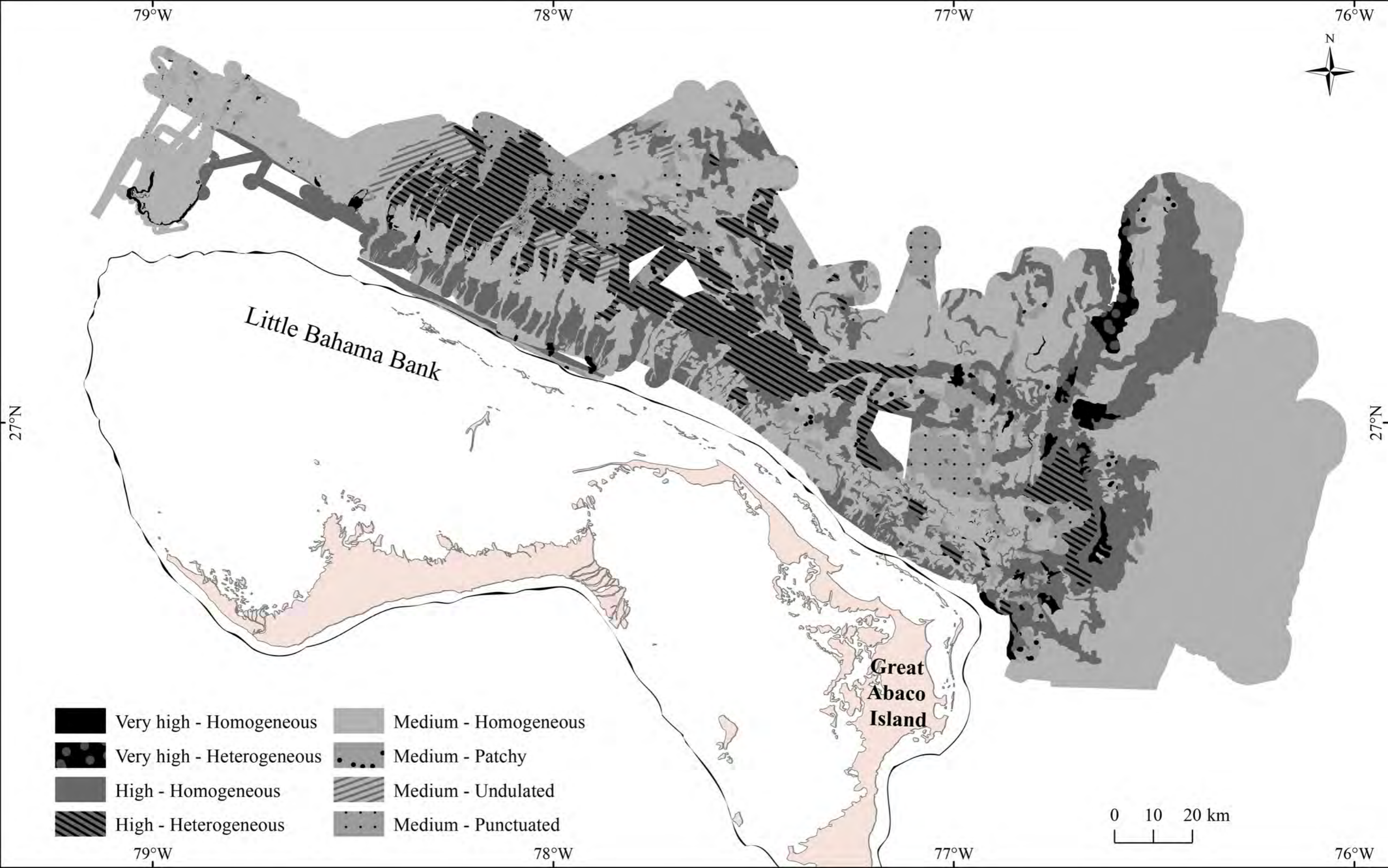




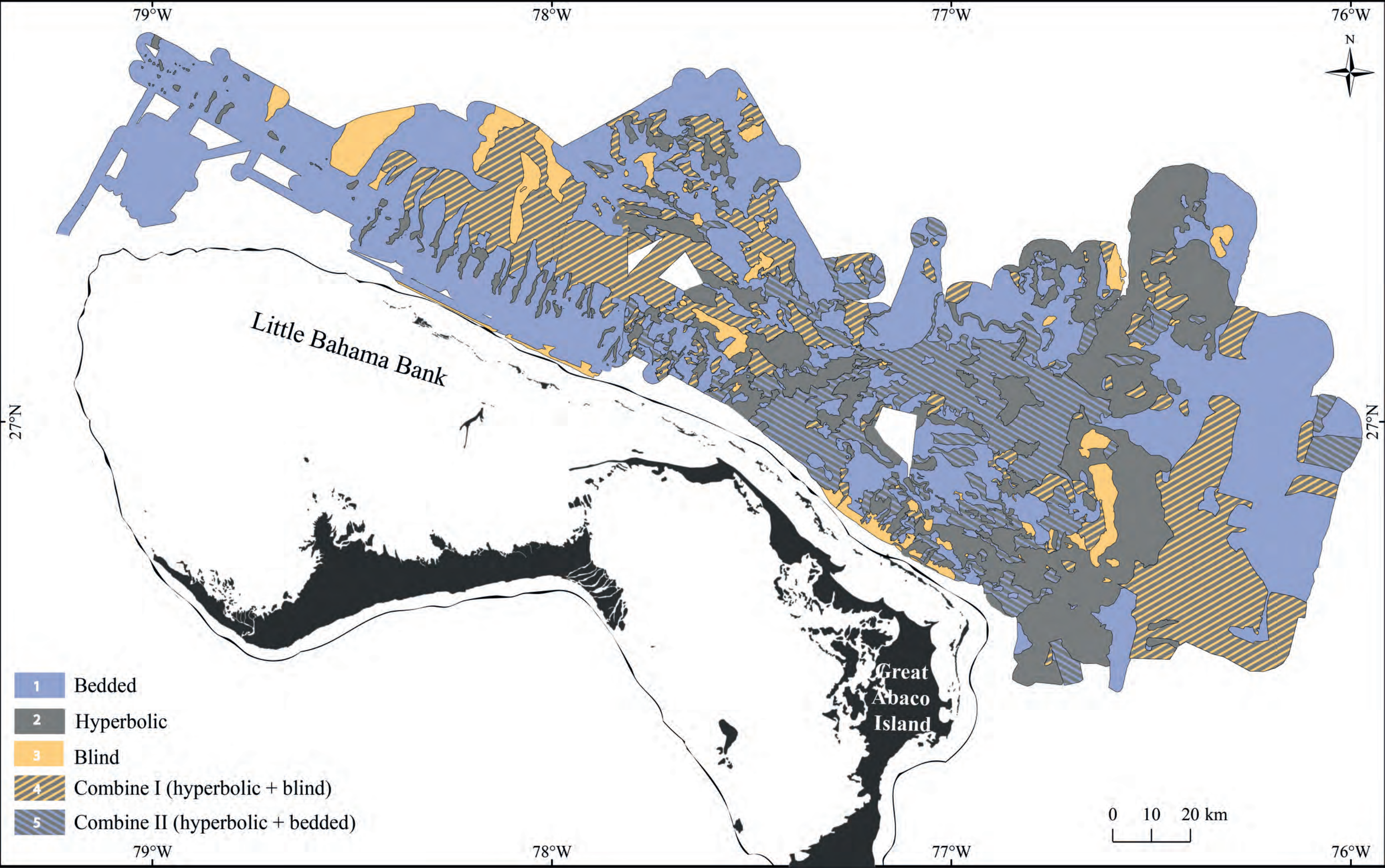




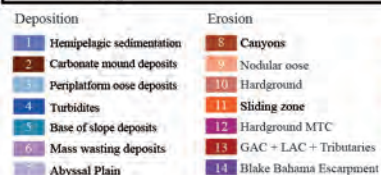
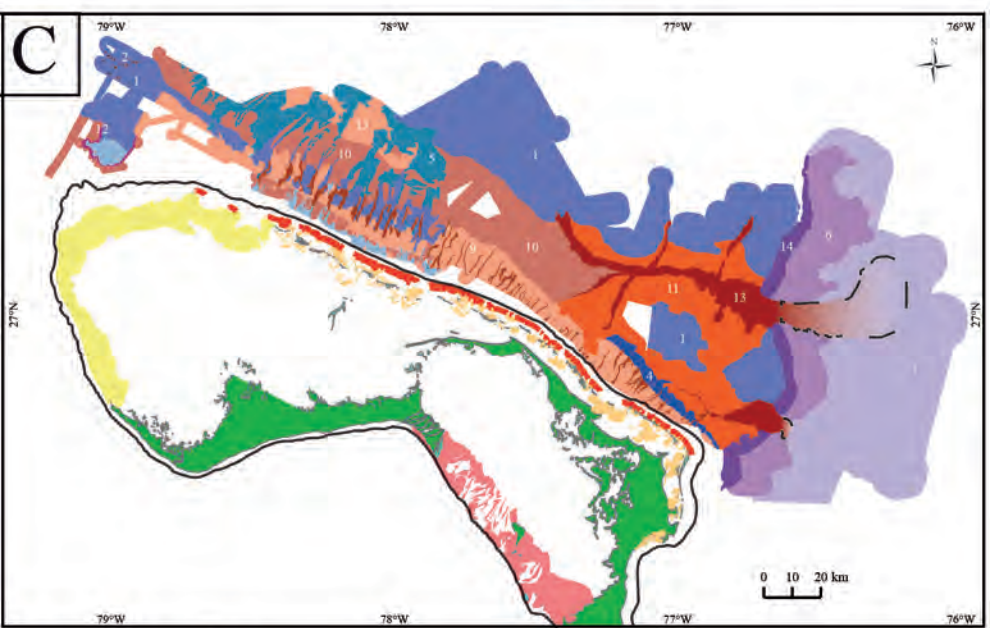
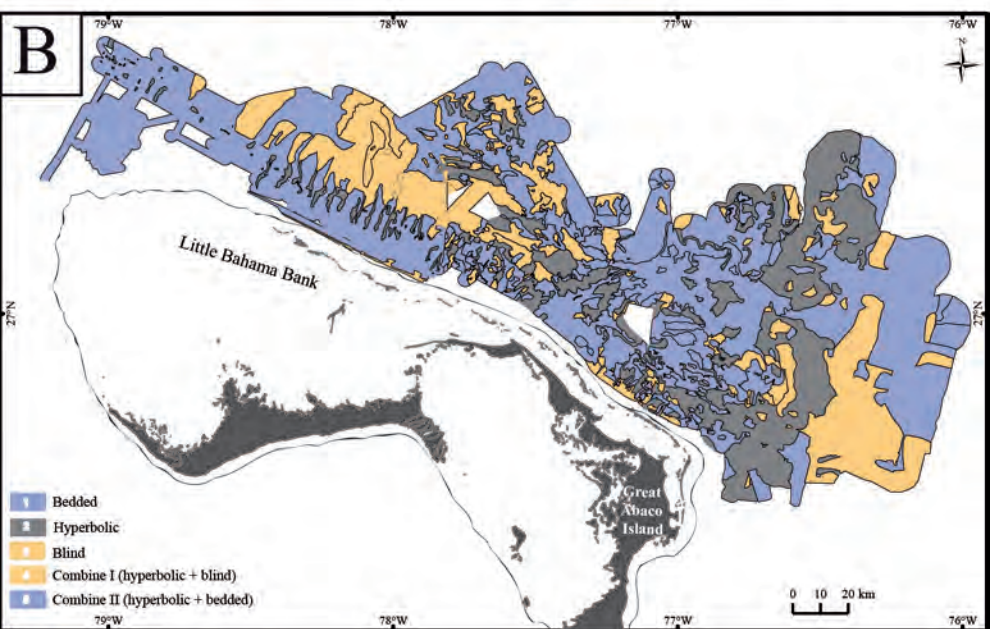
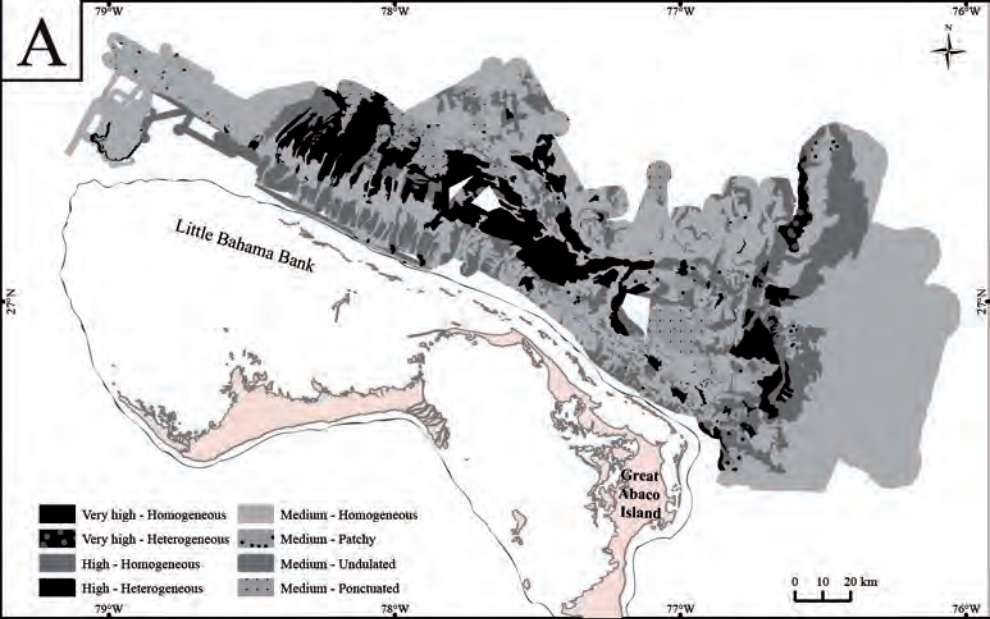




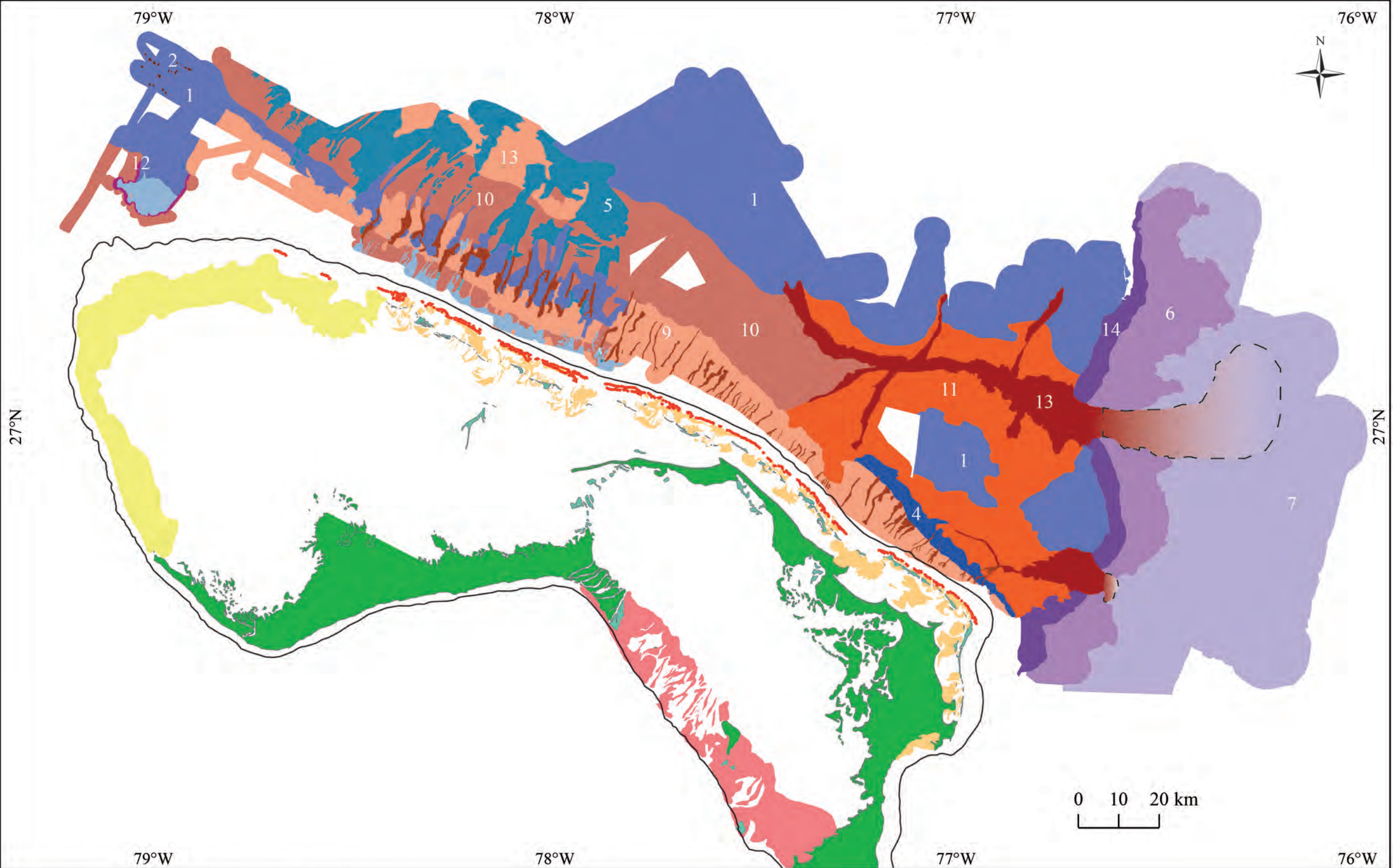












### Deposition

- 1 Hemipelagic sedimentation
- 2 Carbonate mound deposits
- 3 Periplatform ooze deposits
- 4 Turbidites
- 5 Base of slope deposits
- 6 Mass wasting deposits
- 7 Abyssal Plain

### Erosion

- 8 Canyons
- 9 Nodular ooze
- 10 Hardground
- 11 Sliding zone
- 12 Hardground MTC
- 13 GAC + LAC + Tributaries
- 14 Blake Bahama Escarpment

- Reefs
- Marine Sand Belt
- Marine Sand Belt-Tidal Delta
- Tidal Bar Belt
- Island
- - - Lobe



